Establishing a Calibration for a Microwave Plasma
Continuous Emissions Monitor

by

Guadalupe Jorge Flores III

B.S., Nuclear Engineering (1996)
Massachusetts Institute of Technology

Submitted to the Department of Nuclear Engineering
in Partial Fulfillment of the requirements for the Degree of
Master of Science in Nuclear Engineering

at the

Massachusetts Institute of Technology

June 1998

© 1998 Massachusetts Institute of Technology

Signature of Author ....

Department of Nuclear Engineering
May 9, 1998

Certified by ....

Paul P. Woskov
Associate Division Head, Plasma Technology Division
Plasma Science and Fusion Center, Thesis Supervisor

Certified by ....

Kenneth R. Czerwinski
Assistant Professor of Nuclear Engineering
Thesis Advisor

Accepted by ....

Lawrence M. Lidsky
Professor of Nuclear Engineering
Chairman, Department Committee on Graduate Students

Science

Establishing a Calibration for a Microwave Plasma Continuous Emissions Monitor

by

Guadalupe Jorge Flores III

Submitted to the Department of Nuclear Engineering
on May 8, 1998 in Partial Fulfillment of the
Requirements for the Degree of Master of Science in
Nuclear Engineering

ABSTRACT

In an effort to provide an accurate real-time continuous emissions monitor (CEM) for hazardous air-pollution metals as a viable option to EPA Method 29, a Microwave Induced Plasma (MIP) system is under development for real-time atomic emission spectroscopy in stack exhaust. This MIP-CEM has a nebulizer calibration subsystem attached to the sample line for real-time span calibration of the monitored metal concentrations. In order to quantify the amount of metal mass measured in the effluent flow, it is necessary to determine the analyte metal mass transport efficiency of the nebulizer system. A novel new approach to determine the nebulizer efficiency during plasma operation was tested in this thesis. A 0.1-mm tungsten filament attached to a 4-mm diameter alumina rod was used to introduce a known amount of mass into a nitrogen plasma at 0.5-cfm sample line flow in 6 different positions relative to the end of the sample line. The tungsten filament was heated by plasma radiation. These signals, obtained from the direct rod insertions, were then correlated to masses of metals aspirated by the nebulizer and drawn into the plasma through a quartz "T". The mass transport efficiency as a function of rod insertion position was calculated by dividing the correlated mass by the total mass aspirated by the nebulizer to achieve an identical signal. In the 4-inch long drift distance between the end of the sample line and the plasma sustaining waveguide, measurements from 0.5 inches away from the end of the sample line to 1.75 inches away, in 0.25-inch increments, were repeated, and the results tabulated. The efficiencies generally decreased as the rod was inserted closer to the plasma, with the efficiency extrapolated to 0.644 ± 0.153 % at the end of the sample line. The extrapolated value is in fair agreement with the efficiency used in the most recent field test conducted at Research Triangle Park in Raleigh-Durham, North Carolina. Initial tests at one insertion location of 1.75 in. were also done for a different nitrogen flow of 1.0 cfm and for air at 0.5 cfm. These initial tests are inconclusive, and more measurements are needed. Also, further testing is warranted for the determination of other factors, such as moisture, and the impact on the efficiency.

Thesis Supervisor: Dr Paul P. Woskov
Title: Associate Division Head, Plasma Technology Division,
     Plasma Science and Fusion Center, Massachusetts Institute of Technology

Acknowledgements

Where to begin? Who to thank? It almost as if I am writing my acceptance award for the Oscars. But oh well, here goes my version of it.

I would like to thank Dr. Paul P. Woskov for giving me the opportunity to work and learn in the group. I feel that I have learned so much from just going in head first and doing the job, and I appreciate his time, understanding, and patience in letting me learn at my own pace.

I would like to thank Paul Thomas and Bill Keating for their invaluable technical expertise, as well as their friendly advice on the Institute, and how things get done around here. Not to mention fabricating most of the parts that make up the torch and therefore allowing me to test at all.

For taking a fresh face and reading his thesis in such a short time, I would like to thank Prof. Kenneth Czerwinski for helping out a struggling graduate student with his friendly demeanor and wit. Not to mention Big Red, for all his help in editing and revising this work you see before you.

For his input in the testing procedure, and his incredible knack to push forward any project he is on, I would like to thank Dr. Kamal Hadidi for acting as a motivator and for his sense of humor. Not to mention his desire to show me the inner workings of any computer he came into contact with.

Friends, lab partners, classmates; all of these describe Karyn Green and Brian Pollack. These two people have probably had more contact with me than anyone else has in my tenure here as a graduate student, and I could not ask for better lab partners anywhere. Karyn, with her meticulous nature, has shown me that sometimes it's the

details that really count and what it means to really do research. Brian took a guy who never used a wrench in any serious manner before and taught him how to assemble pipes and other cool stuff like that. Both taught me how to have fun in lab; these two people have left very special imprints in the way I approach my studies and life here at the Institute.

To all my family at home, Mom, Dad, and Robert, wherever they may be, I owe then thanks, for they have, in their own separate ways, each shown me something about the person I am on the road to becoming. It had not been an easy year for my family, but we have prevailed, and in writing this thesis, I take some of that strength and love, and preserve it for all time.

And finally, to the one I hold most dear to my heart, my significant other, Angela Leverich. What can I say? She listened to me complain, and rejoiced at the little triumphs in lab. She is my best friend, and so much more, and I hope to spend a lot of time finding out just how much more important she will be in my life.

To all those mentioned here, you have my heart-felt thanks. Each of you, I your own way, has contributed something to this thesis, and more importantly, to the author. I would like, however, to dedicate this to my family, present, and future. May I strive to be worthy of the love I have been given.

Well, enough of this. I have to finish this, and start studying for the qualifying exam in September. Hopefully, I will have a few more years with the group, and I look forward to new and exciting challenges in all parts of my life.

Here goes nothing!

Table of Contents

List of Figures and Tables

1.0 Introduction

This thesis is a continuation of the work being done at the Massachusetts Institute of Technology Plasma Science and Fusion Center on a microwave plasma torch for real-time multi-metals monitoring.

1.1 Thesis Motivation

The goal of this thesis is to determine the aerosol generation and analyte mass transport efficiency of the nebulizer subsystem used to calibrate the plasma torch system used at the Environmental Protection Agency (EPA) Research Center located in Research Triangle Park, Durham, North Carolina. This will involve simulating the flow conditions at that test, determining which factors can not accurately be modeled, and describing the impact on this analysis.

A calibration scheme will be designed and implemented based on the working conditions recorded at the test site, using direct rod insertions of known quantities of metals as reference. Once completed, the nebulizer subsystem will be activated and the mass transport efficiency calculated. This procedure will be repeated for several different rod positions in the plasma chamber, and the transport efficiency tabulated for these positions will determine the efficiency at the end of the sample line.

1.2 Information to Follow

Chapter 2 deals with the motivation for this calibration, as well as the current monitoring system and several alternatives to this type of system. A basic theoretical discussion of spectroscopy is outlined in this chapter. Chapter 3 deals with the physical aspects of the entire system, with emphasis on the nebulizer setup and spectrometer workings. The technical aspects of plasma formation are also discussed in this chapter. Chapter 4 deals with the calibration scheme and its motivation. The mass transport efficiency will be defined and discussed in further detail. The effects of sample concentration on the efficiency will also be examined and its impact determined. Chapter 5 will deal with the analysis of the data, including an error analysis. Data from several positions will be presented, as well as several tests showing the flexibility of the calibration scheme. Finally, chapter 6 will summarize the work up to date, and conclusions will be drawn. Recommendations for future work will also be discussed.

2.0 Background

2.1 EPA Regulations and CEMS Requirements

2.1.1 EPA Regulations and Detection Limits

The Environmental Protection Agency (EPA) has recently made more stringent restrictions in the emissions standards of 17 hazardous elements released from stationary sources. New emissions limits have been set on antimony (Sb), arsenic (As), barium (Ba), beryllium (Be), cadmium (Cd), chromium (Cr), cobalt (Co), copper (Cu), lead (Pb), manganese (Mn), mercury (Hg), nickel (Ni), phosphorus (P), selenium (Se), silver (Ag), thallium (Tl), and zinc (Zn).

The existing limit on Pb and Cd combined was 270 μg/dscm, (dry standard cubic meter), while the new regulations call for a limit of 62 μg/dscm. The limit for low volatility metals (As, Be, Cr, Sb) combined was 210 μg/dscm, while the new limit calls for less than 80 μg/dscm if a continuous emissions monitoring system is used. However, the limit for Hg has not been changed, and remains at 50 μg/dscm. [1]

According to Performance Specification 10, "Specifications and Test Procedures for Multi-Metals Continuous Monitoring Systems in Stationary Sources", a continuous emissions monitoring system (CEMS) is defined as "the total equipment required for the determination of a metal concentration." There are two types of CEMS defined in the specification: Point CEMS and Path CEMS, depending on the sampling area. A point CEMS samples either a single point in the duct, or less than 10 percent of the equivalent diameter of the duct. A path CEMS samples over 10 percent of the equivalent diameter

---

[1] U. S. EPA, Revised Standards for Hazardous Waste Combustors, Performance Specification 10 – Specifications and Test Procedures for Multi-Metals Continuous Monitoring Systems in Stationary Sources, pp. 2-3.

of the duct, where the equivalent diameter is equal to 4 times the cross sectional area

divided by the wetted perimeter, as shown in equation 2.1.

$$D_{eff} = \frac{4 \times A}{P_{wetted}} \qquad (2.1)$$

2.1.2 CEMS Subsystems

For either CEMS system, there are four major subsystems that the CEMS must

possess, defined below:

> 1) The Sample Interface is the part of the CEMS that makes physical
>
> contact with the emissions, whether gathering, transporting, or preparing
>
> the sample for analysis
>
> 2) The Pollutant Analyzer is the subsystem that does the actual breakdown
>
> of the effluent gas to determine the metals concentrations, and generates
>
> an equivalent output that can be interpreted for the results in question.
>
> 3) The Diluent Analyzer determines how much extra gas was added in the
>
> process of gathering the sample, and generates a signal that can be used to
>
> take the extra gas in the sample into account for the final analysis.
>
> 4) The Data Recorder makes some form of physical permanent record of
>
> the signals generated by the system for analysis by the operators.[2]

2.1.3 CEMS Requirements

In addition to having these four subsystems, there are seven other specifications to

which a CEMS system must conform.[3]

---

[2] U. S. EPA, Revised Standards for Hazardous Waste Combustors, Performance Specification 10 – Specifications and Test Procedures for Multi-Metals Continuous Monitoring Systems in Stationary Sources, p. 627.

[3] Ibid., pp. 629-640.

1) Measurement location. The CEMS should be placed at least eight equivalent diameters downstream of any source of flow instabilities, such as bends or extra pollution sources, and at least two equivalent diameters upstream of any effluent exhaust.

2) Data Recorder Scale. The CEMS data recorder should include a zero level, and should be able to read 20 times the acceptable limit for each metal sampled. In addition, it must be able to switch between any lower values and this maximum value at any time in the measurement.

3) Relative Accuracy: The CEMS must have a relative accuracy no greater than 20 % of the reference method values, where the relative accuracy is calculated by equation 2.2,

$$RA = \frac{\overline{d} + \frac{t_{0.975}}{\sqrt{n}} SD}{\overline{R}_{RM}} \qquad (2.2)$$

where $\overline{d}$ is the arithmetic mean of the difference in the data for the CEMS and the reference method, $\overline{R}_{RM}$ is the average of the reference method data set, defined in equation 2.3,

$$\overline{R}_{RM} = \frac{1}{n} \sum_{i=1}^{n} R_{RM,i} \qquad (2.3)$$

n is the number of points in the data set, $t_{0.975}$ is the t-value at 2.5 percent error confidence read from table 2.1,

n	$t_{0.975}$	n	$t_{0.975}$	n	$t_{0.975}$
2	12.706	7	2.447	12	2.201
3	4.303	8	2.365	13	2.179
4	3.182	9	2.306	14	2.160
5	2.776	10	2.262	15	2.145
6	2.571	11	2.228	16	2.131

Table 2.1 $t_{0.975}$ Values

and SD is the standard deviation of $\bar{d}$ calculated from equation 2.4.

$$SD = \sqrt{\frac{\sum_{i=1}^{n} x_i^2 - \frac{1}{n}\left(\sum_{i=1}^{n} x_i\right)^2}{n-1}} \qquad (2.4)$$

4) Drifts. The CEMS must take into account calibration and zero value drift in the process of measuring the emissions during a test run. The calibration and zero drifts may not exceed more than 5 % of the emission limit for each metal. Calibration should be done at points that are at least 80 to 120 % the emission limit for each metal. The zero drift tests will be done with a calibration solution that is up to 20 % of the emission limit for the metal in question. The calibration drift, in %, is given by equation 2.5,

$$CD = \frac{R_{CEM} - R_V}{R_V} \times 100 \qquad (2.5)$$

where R_{CEM} is the value of the data of the CEMS, and R_V is the value of the data referenced at the high calibration level. The zero drift, also in %, is given by equation 2.6,

$$ZD = \frac{R_{CEM} - R_V}{R_{EM}} \times 100 \qquad (2.6)$$

where, again, R_{CEM} is the value of the CEMS data, R_V is the value referenced at the low calibration level, and R_{EM} is the emissions limit for the metal.

5) Sampling and Response Time. For an instantaneous CEMS, the response time should be no more than 2 minutes for the data value to reach 95 % of the final stable value, while sampling continuously.

6) Measurement of Relative Accuracy. For all tests, note the exact time of day each test was started and completed. The CEMS and the reference method must be run at a single level for each metal tested. Also, for one metal, there will be three tests done, one at 0 to 20 %, one at 40 to 60 %, and one at 80 to 120 % of the emission limit for that metal. There will be three tests done for each metal at each of the three levels, for a total of nine pair of measurements per metal. Testing conditions should be as similar as possible, with regards to position, moisture loading, etc.

7) Reporting. The results of the calibration drift and the relative accuracy tests should be reported in tabular form. All calculations, data sheets, and other records should also be reported. All CEMS measurements should be made in $\mu g/m^3$ on a dry basis at 20° C and 7 % O_2.

As of March 22, 1995, Method 29 is the only multi-metal reference method approved for comparison tests for stationary sources. The next section will describe Method 29 in greater detail.

2.2 Method 29

Method 29, Determination of Metals Emissions from Stationary Sources is described in explicit detail in 40 CFR 60 Part A in the Code of Federal Regulations. Method 29 can monitor all 17 metals mentioned above, although there are several complications when it comes to the mercury analysis. Method 29 isokinetically samples the effluent gas and draws the sample through a set of filters and impingers, where the

sample is extracted and prepared for analysis by several different means. A diagram of

Method 29 is shown below.
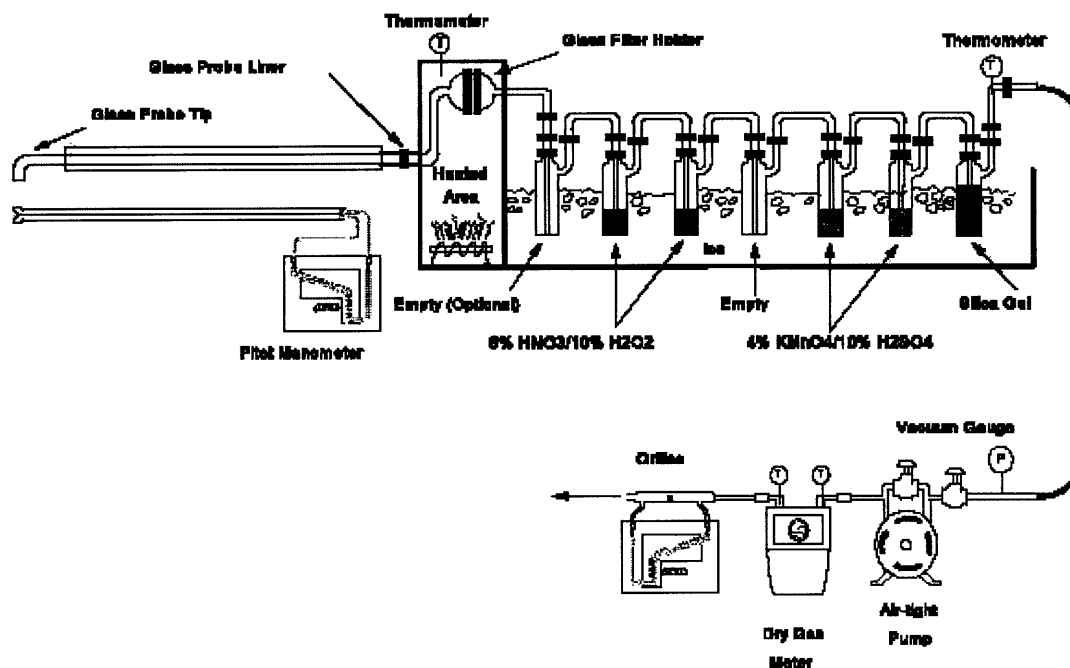
Figure 2.1 Overview of Method 29 Setup [4]

Each phase of Method 29 will be discussed in further detail in the succeeding sections.

In the writeup for Method 29, another test is often referenced. Method 5-Determination

of Particulate Emissions from Stationary Sources, is also located in the Code of Federal

Regulations, in 40 CFR 60 Appendix A, and is referred to for specific details common to

both systems.

2.2.1 Stack Sampling

Method 29 employs a quartz probe that is heated to maintain an exit gas

temperature of 120 ± 14 °C.[5] The probe samples the effluent gas isokinetically to ensure

---

[4] U. S. EPA, Method 29, <u>Determination of Metals Emissions from Stationary Sources,</u> p.7.

[5] U. S. EPA, Method 5, <u>Determination of Particulate Emissions from Stationary Sources</u>, p. 543.

a representative sample of metals concentration. Isokinetic sampling means that the probe suction velocity is matched to the local freestream velocity in the area that sampling is occurring. This constraint guarantees a representative sampling of the duct, since the probe will not draw or deflect particles that are on streamlines away from the critical streamlines intersecting the cross sectional area of the probe.[6]
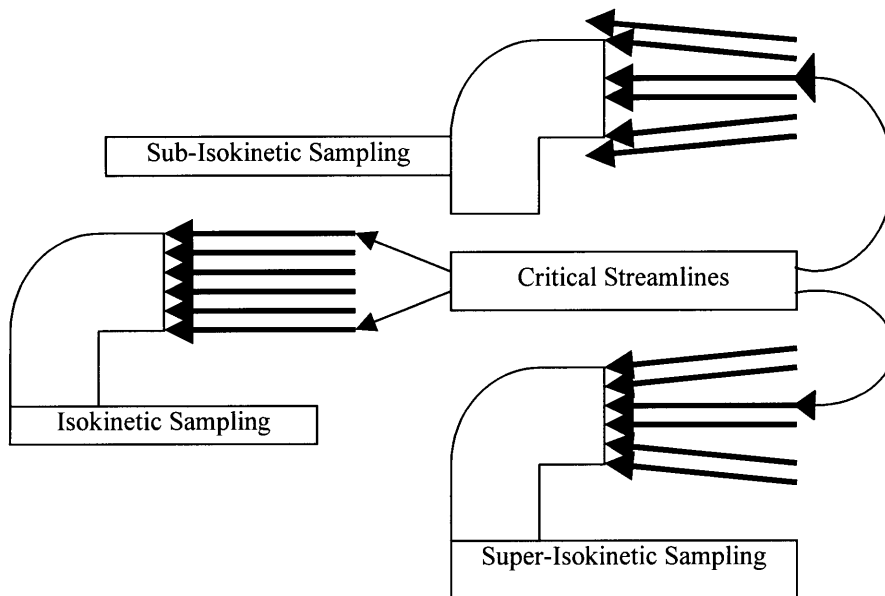
Figure 2.2 Comparison of Streamlines for Sampling Isokinetically

2.2.2 Preparation for Sampling

Method 29 uses 7 impingers with three different solutions to capture the sample, along with quartz or glass fiber filters upstream of the impingers. The first capturing device is the filter, which should be desiccated and weighed if particulate emissions are monitored. The extensive amount of glassware must be rinsed in hot tap water, washed in hot soapy water, and rinsed in water three times. Then the glassware is soaked in a 10 % V/V solution of nitric acid/water for at least 4 hours, at which time it is rinsed another three times in water, and then in acetone, at which time it is allowed to air dry. The

---

[6] Pollack, Brian, Establishing Isokinetic Flow for a Plasma Torch Exhaust Gas Diagnostic for a Plasma Hearth Furnace, p. 21.

glassware must be covered until assembly. In addition, a solution of 5 % HNO$_3$/10 % H$_2$O$_2$ solution and a solution of 4 % KMnO$_4$ (WV)/10 % H$_2$SO$_4$ (V/V) must be prepared for the sample line. Detailed instructions and amounts of material used are given in the write-up for Method 29. All solutions must contain less than 2 ng/ml of the target metal. In addition, an extensive leak-check procedure on the sample train must be performed before each run.[7]

2.2.3 Sampling Train Operation

As the sampling train is in operation, there are several things to maintain. The gas temperature should be 120 ± 14°C at the filter, and the sampling rate should be within 10 % of true isokinetic sampling. Leak test procedures must be implemented as the test is occurring. The impingers must be maintained at the correct temperature of 20° C by adding ice and salt to the impinger housing assembly. The probe must sample several points along the length of the stack cross section; one sampling train must be used for each sample run. The exact details for train operation are given in the Method 29 write-up.[8]

2.2.4 Calculation of Percent Isokinetic

In order to determine if a run is acceptable for analysis, the operators must calculate how close to true isokinetic sampling the system operates. Equation 2.7, given in Method 5, shows how to calculate I, the percent isokinetic, from the raw data.

$$I = \frac{100 \cdot T_S [K_3 V_{lc} + (\frac{V_M Y}{T_M})(P_{bar} + \frac{\Delta H}{13.6})]}{60 \Theta v_s P_s A_n} \tag{2.7}$$

---

[7] U. S. EPA, Method 29, <u>Determination of Metals Emissions from Stationary Sources</u>, pp.15-16.

[8] Ibid., p. 16.

For a run to be valid, I must be in the range of 90 % to 110 %; if not, the test must be re-run until I falls within the proper range. The terms are described below: [9]

> T_S is the absolute average stack temperature [K],
> $K_3 = 0.003454$ mmHg-m^3/ml-K,
> V_{lc} is the total volume of liquid collected in the impingers and silica gel [ml],
> V_M is the volume of gas sampled as measured by the dry gas meter [dcm],
> Y is the dry gas meter calibration factor,
> T_M is the absolute average dry gas meter temperature [K],
> P_{bar} is the barometric pressure at the sampling point [mmHg],
> ΔH is the average pressure differential across the orifice meter [mmH$_2$O],
> 13.6 is the specific gravity of Hg,
> Θ is the run time [min],
> v_s is the stack gas velocity [m/sec],
> P_s is the absolute stack gas pressure [mmHg], and
> A_n is the cross sectional area of the nozzle [m^2]

Once the test has been deemed acceptable, sample recovery is the next priority.

2.2.5 Sample Recovery

Once the run has been certified acceptable, the sample must be removed and prepared for analysis. Among the many steps in this phase is the cleanup of the probe and the removal of the filters. Sample recovery should be done in a place that is free of contaminants. The following flowchart outlines the recovery scheme.

---

[9] U. S. EPA, Method 5, Determination of Particulate Emissions from Stationary Sources, p.558.

Probe Liner and Nozzle	Front Half of Filter Housing	Filter	Filter Support and Back Half of Filter Housing	1st Impinger (Empty at start of test)	2nd and 3rd Impingers (HNO₃/H₂O₂)	4th Impinger (Empty) and 5th and 6th Impingers (Acidified KMnO₄)	Last Impinger

Figure flowchart:

- **Probe Liner and Nozzle** → Rinse with acetone → Brush liner with nonmetallic brush and rinse with acetone → Check liner t see if particulate removed, if not, repeat step above → Rinse three times with 0 1 N HNO₃ → **FH (3)**
- **Front Half of Filter Housing** → Brush with nonmetallic brush and rinse with acetone → Rinse three times with 0 1 N HNO₃ → **AR (2)**
- **Filter** → Carefully remove filter from support with Teflon coated tweezers and place in petri dish → Brush loose particulate onto filter → Seal petri dish with tap → **F (1)**
- **Filter Support and Back Half of Filter Housing** → Rinse three times with 0 1 N HNO₃
- **1st Impinger (Empty at start of test)** → Measure impinger contents → Empty contents into container → Rinse three times with 0 1 N HNO₃ → **BH (4)**
- **2nd and 3rd Impingers (HNO₃/H₂O₂)** → Measure impinger contents → Empty contents into container → Rinse three times with 0 1 N HNO₃ → **0 1 N HNO₃ (5A)**
- **4th Impinger (Empty) and 5th and 6th Impingers (Acidified KMnO₄)** → Measure impinger contents → Empty Impinger No 4 contents into container → Rinse with 100 ml 0 1 N HNO₃ → **KMnO₄ (5B)** ; Empty Impinger Nos 5 & 6 contents into container → Rinse three times with permanganat reagent, then with water → Remove any residue with 25 ml 8N HCl solution → **8 N HCl (5C)**
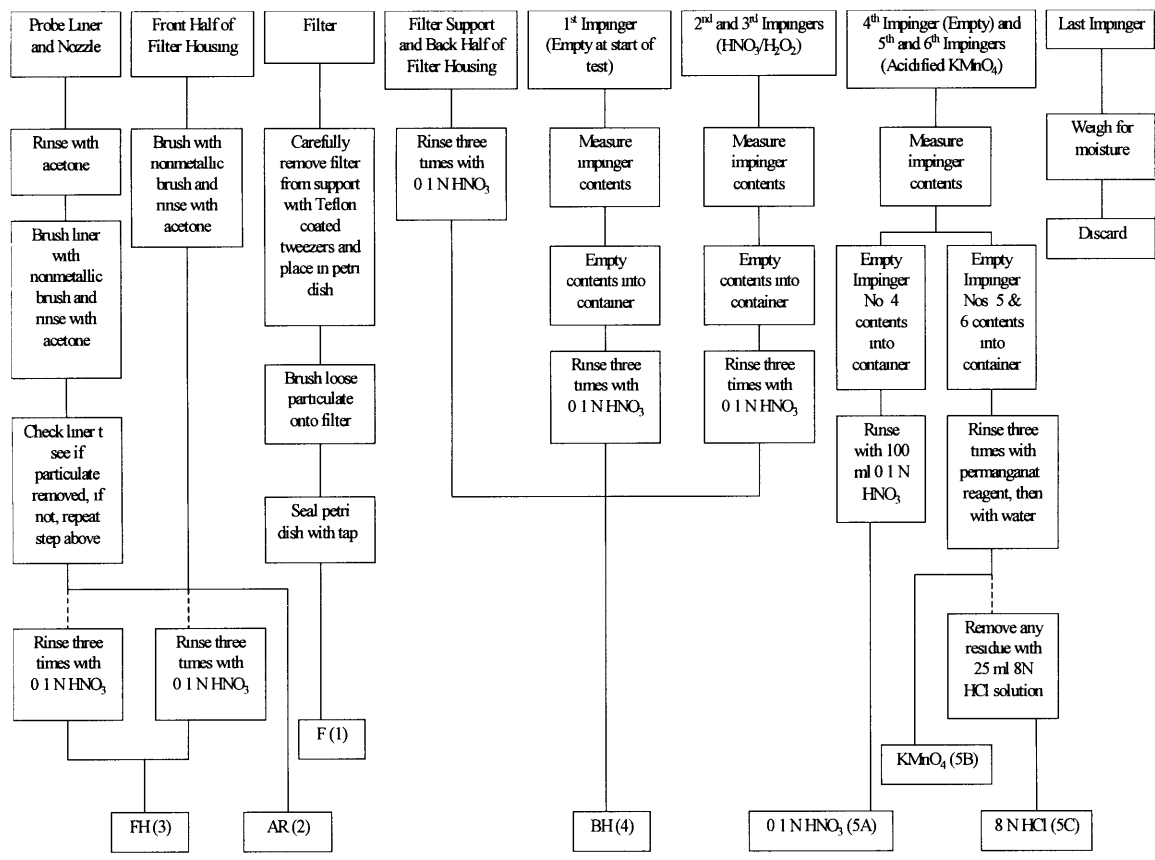- **Last Impinger** → Weigh for moisture → Discard

Figure 2.3 Method 29 Sample Recovery Scheme [10]

As seen from the chart, there are 7 samples that need to be analyzed. The sample preparation and analysis scheme will be presented in the next section.

2.2.6 Sample Preparation and Analysis

The analysis continues along the same track as the preparation; these 7 new samples must further be digested and broken down before the actual analysis can be done. The analysis done actually depends on the target metal, as listed below:

1) Cold Vapor Atomic Absorption Spectroscopy (CVAAS)--Hg only
2) Inductively Coupled Argon Plasma Spectroscopy (ICAP)--Sb, As, Ba, Be, Cd, Cr, Co, Cu, Pb, Mn, Ni, P, Se, Ag, Tl, and Zn
3) Atomic Absorption Spectroscopy (AAS)—same metals as ICAP
4) Graphite Furnace Atomic Absorption Spectroscopy (GFAAS)--Sb, As, Cd, Co, Pb, Se, and Tl if a greater sensitivity is needed than ICAP
5) Inductively Coupled Plasma-Mass Spectroscopy (ICP-MS)—Sb, As, Ba, Be, Cd, Cr, Co, Cu, Pb, Mn, Ni, As, Tl, and Zn

---

[10] U. S. EPA, Method 29, Determination of Metals Emissions from Stationary Sources, pp. 18-19.
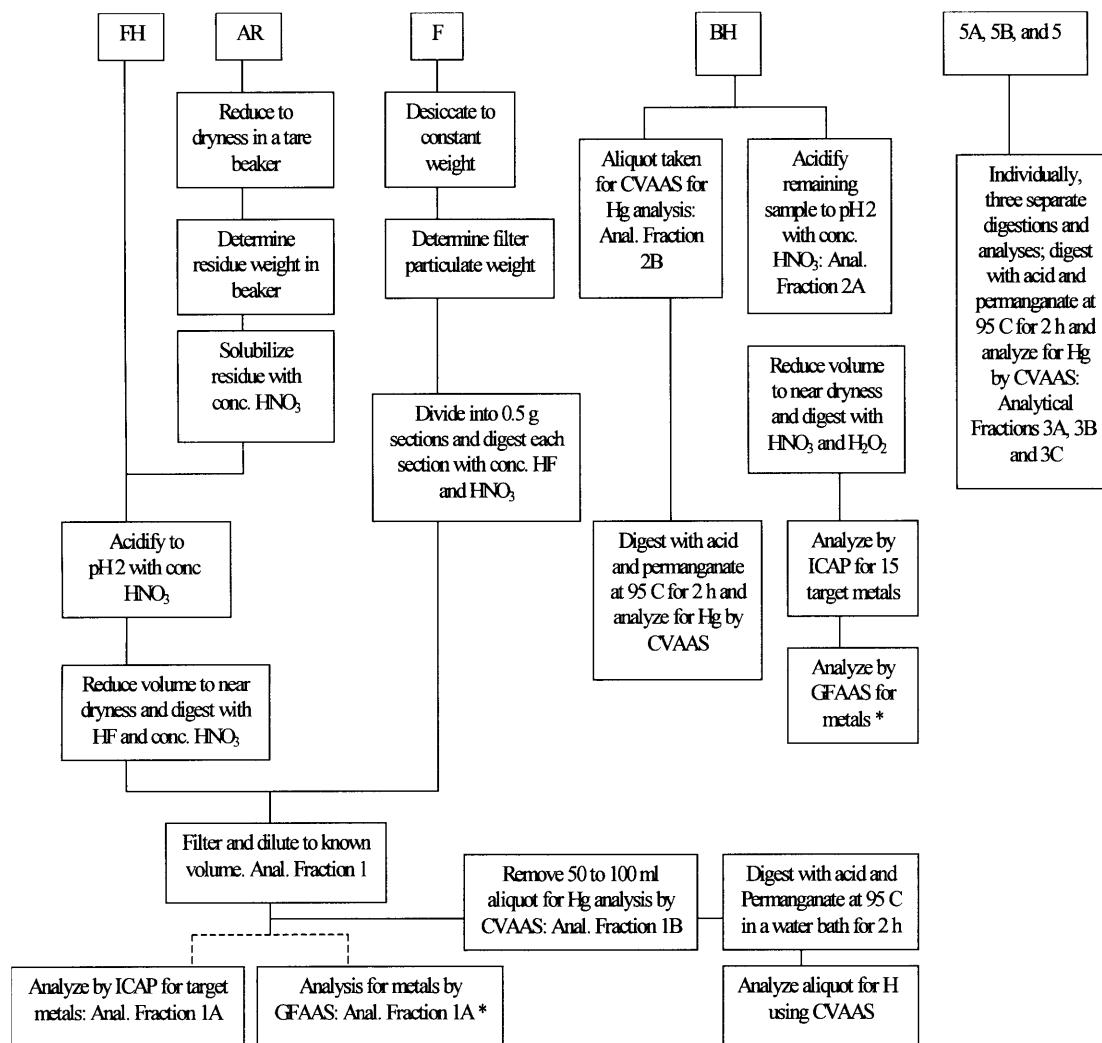
The total scheme is given below.

Figure 2.4 Method 29 Sample Preparation and Analysis Scheme[11]

The lettered start boxes are those samples prepared from the recovery scheme, Figure 2.3.

Those processes with an asterisk denote analysis by AAS for metals with concentrations

less than 2 μg/ml in digestate solution, where ICAP is not sensitive enough for the

analysis. The limits for detection are given in the next section.[12]

---

[11] U. S. EPA, Method 29, Determination of Metals Emissions from Stationary Sources, p. 26.

[12] Ibid., p.32.

2.2.7 Calculations and Detection Limits

The calculation for individual concentrations of the metals in the stack is rather straightforward. The difficulty comes in determining the masses and volumes of all the analytical fractions involved in the process. The concentration is determined by the following procedure.

2.2.7.1 Calculation of Dry Gas Volume

The sample volume measured with the dry gas meter must be corrected to 1 atmosphere at 20 °C by equation 2.8,[13]

$$V_{m(std)} = V_m Y \left(\frac{T_{std}}{T_m} \right) \left[\frac{P_{bar} + \dfrac{\Delta H}{13.6}}{P_{std}} \right] = K_1 V_m Y \frac{P_{bar} + \left(\dfrac{\Delta H}{13.6} \right)}{T_m} \tag{2.8}$$

where K_1=0.3858 K/mmHg, P_{std}=760 mmHg, T_{std}=293 K,
V_M is the volume of gas sampled as measured by the dry gas meter [dcm],
Y is the dry gas meter calibration factor,
T_M is the absolute average dry gas meter temperature [K],
P_{bar} is the barometric pressure at the sampling point [mmHg],
ΔH is the average pressure differential across the orifice meter [mmH$_2$O],
13.62 is the specific gravity of mercury

2.2.7.2 Calculation of Volume of Water Vapor and Moisture Content

The total volume of condensate in the train and the moisture content of the sample gas must be determined for corrections to the signal and for correlation to other tests. The condensate volume is given by equation 2.9:

$$V_{w(std)} = \frac{V_{lc} \rho_w R T_{std}}{M_w P_{std}} = K_2 V_{lc} \tag{2.9}$$

---

[13] U. S. EPA, Method 5, <u>Determination of Particulate Emissions from Stationary Sources</u>, p.557.

where R=0.06236 mmHg-m^3/K-g-mole, P_{std}=760 mmHg, T_{std}=293 K, ρ_w=1.0 g/ml,

M_w=18.0 g/g-mole, K_2=0.001333m^3/ml, and V_{lc} is the total volume of liquid collected in

the impingers and the silica gel.[14]

2.2.7.3 Metals in Source Sample: Analytical Fraction 1A and 2A

For each metal, use equation 2.10 to calculate the concentration of each metal in

Sample Fraction 1 or 2, as defined in Figure 2.4:

$$M_{[fh],[bh]} = C_{[a1],[a2]} F_{[d],[a]} V_{[so\,ln,1],[a]} \qquad (2.10)$$

where the terms are defined:

$M_{[fh],[bh]}$ = total mass of metal, except Hg, collected in the front or back half of the train [μg],
$C_{[a1],[a2]}$ = concentration of metal in Analytical Fraction 1A or 2A [μg/ml],
$F_{[d],[a]}$ = dilution factor (inverse of the fractional portion of the concentrated sample in the solution actually used in the instrument to produce the reading C_{a1}) or aliquot factor (volume of Sample Fraction 2 divided by volume of Sample Fraction 2A)
$V_{[soln,1],[a]}$ = total volume of digested sample solution in Analytical Fraction 1 or 2A [ml][15]

2.2.7.4 Metals in Total Train, Except Hg

The analysis for the total train is a linear superposition of the two fractional

analyses, with a correction factor added in, demonstrated by equation 2.11:

$$M_t = \left(M_{fh} - M_{fhb}\right) + \left(M_{bh} - M_{bhb}\right) \qquad (2.11)$$

where

M_t = total mass of each metal collected in sampling train [μg],
M_{fhb} = the blank correction value for metal detected in front half field reagent blank. If $0.0 < M_{fhb} < (1.4\ \mu g/in2 * $ sample filter area), then use the value of M_{fhb} to correct the mass value. If $M_{fbh} > (1.4\ \mu g/in2 * $ sample filter area), then use the larger value of either (1.4 mg/in2 * sample filter area) or the lesser value of M_{fhb} and 5 percent of M_{fh}. [μg]

---

[14] U. S. EPA, Method 5, Determination of Particulate Emissions from Stationary Sources, p.557.

[15] U. S. EPA, Method 29, Determination of Metals Emissions from Stationary Sources, p. 40.

M_{bhb} = the blank correction value for metal detected in back half field reagent blank. If $0.0 < M_{bhb} < 1.0$ μg, then use M_{bhb}. If $M_{bhb} > 1.0$ μg, then use either the greater value of 1.0 μg or the lesser value of M_{bhb} and 5 percent of M_{bh}. [μg][16]

2.2.7.5 Hg in Total Train

The Hg analysis follows exactly the same pattern, except that there are more fractions to analyze. The blank correction values also slightly differ from these listed above, but these will not be discussed. It is sufficed to say that the analysis follows from the above discussion.[17]

2.2.7.6 Individual Metals Concentrations in Stack Gas

The final concentrations are determined by the following formula, which is similar to Equation 2.10 in form:

$$C_s = \frac{K_4 M_t}{V_{m(std)}} \qquad (2.12)$$

where $K_4 = 10^{-3}$ mg/μg, and
 C_s = the concentration of a metal in the stack gas, mg/dscm,
 M_t = the total mass of that metal collected in the sample train, μg,
 $V_{m(std)}$ = the volume of gas sample measured by the dry gas meter and corrected to dry standard conditions, dscm[18]

2.2.8 Detection Limits

The Detection limits for Method 29 were calculated using the simple formula:

$$A \times \frac{B}{C} = D \qquad (2.13)$$

where A is the analytical detection limit [μg/ml], B is the liquid volume of digested sample prior to aliquotting for analysis [ml], C is the stack sample gas volume [dscm],

---

[16] U. S. EPA, Method 29, Determination of Metals Emissions from Stationary Sources, p. 40.

[17] Ibid., pp. 41-43.

[18] Ibid., pp. 43-44.

and D is the in-stack detection limit [μg/m³]. The detection limits can be summarized in

the following table:

Metal	Front-Half: Probe and Filter	Back Half: Impingers 1-3	Back Half: Impingers 4-6[2]	Total Train
Antimony	[1]7.7 (0.7)	[1]3.8 (0.4)		[1]11.5 (1.1)
Arsenic	[1]12.7 (0.3)	[1]16.4 (0.1)		[1]19.1 (0.4)
Barium	0.5	0.3		0.8
Beryllium	[1]0.07 (0.05)	[10].04 (0.03)		[1]0.11 (0.08)
Cadmium	[1]1.0 (0.02)	[1]0.5 (0.01)		[1]1.5 (0.03)
Chromium	[1]1.7 (0.2)	[1]0.8 (0.1)		[1]2.5 (0.3)
Cobalt	[1]1.7 (0.2)	[1]0.8 (0.1)		[1]2.5 (0.3)
Copper	1.4	0.7		2.1
Lead	[1]10.1 (0.2)	[1]5.0 (0.1)		[1]15.1 (0.3)
Manganese	[1]0.5 (0.2)	[1]0.2 (0.1)		[1]0.7 (0.3)
Mercury	[2]0.06	[2]0.3	[2]0.2	[2]0.56
Nickel	3.6	1.8		5.4
Phosphorus	18	9		27
Selenium	[1]18 (0.5)	[1]9 (0.7)		[1]27 (0.8)
Silver	1.7	0.9 (0.7)		2.6
Thallium	[1]9.6 (0.2)	[1]4.8 (0.1)		[1]14.4 (0.3)
Zinc	0.5	0.3		0.8

Mercury analysis only.
[1]Detection limit when analyzed by GFAAS.
[2]Detection limit when analyzed by CVAAS, estimated for Back-half and Total Train.
See Sections 2.2 and 5.4.3. Note: Actual method in-stack detection limits may vary from
these values, as described in Section 2.3.3.

Table 2.2 Detection Limits of Method 29, [μg/m³] [19]

As illustrated and explained, it is a lengthy process that can hardly be constituted as real

time. Even with the possibility of analysis on the site that is being monitored, the

analysis itself takes several hours to prepare and perform. But there are other

technologies looking to replace Method 29, and these will be discussed shortly.

However, the next section will contain a brief discussion on the principles of

spectroscopy itself.

2.3 Spectroscopy

---

[19] U. S. EPA, Method 29, Determination of Metals Emissions from Stationary Sources, pp. 2-5.

When an electron loses energy, it jumps from an excited state back to a state with lower energy, and in the process gives off the excess energy as a photon, characterized by a certain wavelength and frequency. As a function of frequency, the excess energy can be expressed as

$$E_2 - E_1 = h\nu \qquad (2.14)$$

where h = $6.626*10^{-34}$ J*sec, (Planck's constant), and ν is the frequency of the emitted photon, in inverse seconds. Due to the wave nature of photons, this frequency can be related to the wavelength by

$$\lambda = \frac{c}{\nu} \qquad (2.15)$$

where λ is the wavelength, in m, and c is the speed of light, $3.00*10^8$ m/s. Because each element has a unique electronic configuration, each element has a unique set of energy levels, and therefore a unique set of frequencies that the element can emit when it's electrons are excited.

These frequencies, and therefore wavelengths can be separated and detected with a spectrometer. Spectrometers using a diffraction grating are most common. Considering the wave nature of light, there is a path difference between rays incident on adjacent ridges of a diffraction grating, causing the light to change intensity. A principle maximum, or an area of intense brightness, occurs when the path difference between adjacent rays is equal to an integer number of wavelengths, leading to the diffraction equation,

$$n\lambda = d \sin\theta \qquad (2.16)$$

where n is the order of the diffraction, an integer; d is the spacing between ridges; and θ is the angle that the incident light makes with respect to the grating normal. So, given the

element, and thereby the change in energy, and combining this with the geometric characteristics of the diffraction grating, the researcher can tune the grating to look for principle maxima of that element by changing θ. All technologies using atomic emission spectroscopy use these same principles to determine the metals by their spectra, but the difference is in the way these different technologies excite the elements in the first place.[20]

2.4 Competing Technologies

In contrast to the complex chemical analysis done by Method 29, most real time CEMS under development depend on a plasma to excite the electrons of the metal atoms for spectrographic analysis.

The Inductively Coupled Plasma, or ICP, is a common tool in the lab, and has been adapted as a CEMS system. The Navy in conjunction with Thermo Jarrell-Ash has developed an ICP that was also tested at the EPA field test in September. This system was located outside the incinerator building in the parking lot and connected to the stack by a 125-foot sample line. ICPs are sensitive to flow transients and instabilities, as well as the feed gas composition. There are air ICP's under development currently. The difficulty in maintaining a stable plasma is a major shortcoming of these systems.

In addition, due to the sensitivity of the ICP to flow instabilities, a complex isokinetic system must be used to condition the flow to better suit the plasma's inherent instabilities. Long sample lines with bends and restrictions, as well as feed gas

---

[20] A. P. French, and E. F. Taylor, "An Introduction to Quantum Physics", pp. 17-42.

introduction for sample conditioning can lead to large errors in measured quantities, and a need for strict sampling conditions.[21]

Another technology being developed to replace Method 29 is the laser spark plasma, currently being developed by DIAL and Sandia Labs. This technology involves focusing a high power laser into the exhaust gas and creating a plasma directly in the flowstream. While this does lead to true *in situ* measurements, the sampling area is only a few tens of micrometers, and the sampling time is on the order of microseconds. Combining these factors with a low laser pulse rate, it can be shown that the volume of gas monitored by a laser spark system is much less than the amount monitored by Method 29. In addition, the sampling is not truly continuous, and it is a less sensitive system than the MIP.[22]

Another technology used in the September EPA test was an X-ray fluorescence system, currently being developed by CES and Metorex. In this system, the sample is collected on a filter that is withdrawn, and exposed to x-rays. The metals on the filter are excited by the x-rays, and emit light. It is similar to AES, but instead of using a plasma to excite the metal atoms, it uses x-rays. The main drawback to this type of analysis is that it is time consuming, and is hardly real time monitoring.

All of which leads to the microwave induced plasmas, (MIPs). MIPs are more robust, with a lower sensitivity to flow transients and feed gas composition. An MIP can be placed *in situ* for direct isokinetic sampling, and can minimize the amount of sampling line needed for difficult sampling conditions. In addition, MIPs can be less costly than

---

[21] Pollack, Brian, Establishing Isokinetic Flow for a Plasma Torch Exhaust Gas Diagnostic for a Plasma Hearth Furnace, p. 13.

[22] Ibid., pp. 13-14.

ICPs, as MIPs can be constructed with commercially available inexpensive components.

All of these reasons make MIPs an attractive alternative to Method 29, and the next

chapter will describe the physical setup of the MIP used for EPA testing and development

as a CEMS.

3.0 Apparatus

3.1 Physical Setup

The physical setup for the torch system used in the measurements has remained

unchanged for some time, and is shown in Figure 3.1. The torch utilizes a 2.45 GHz

magnetron source nominally operated at 1.5 kW to generate microwaves for sustaining

the plasma. A shorted WR284 rectangular waveguide is used to support the plasma

chamber and to transmit the microwaves to the plasma chamber. These microwaves are

transmitted down the waveguide to its shortened end in a transverse electric field (TE)

mode.
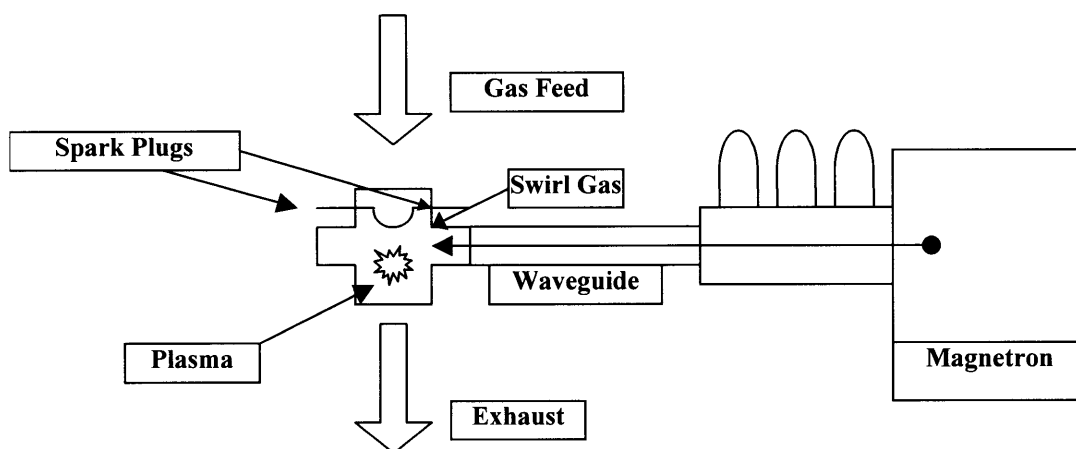
Figure 3.1 Physical Setup of the Plasma Torch

The plasma chamber is created by drilling a hole in the direction of the electric

field ¼ wavelength from the end of the shorted waveguide, where the electric field is at a

maximum.[23] It is through this aperture that a 1-inch I.D. boron nitride dielectric tube is

inserted, creating the plasma chamber and guiding the gas flow through the waveguide.

A primary assembly, which houses the swirl jets and serves as the attachment point for

the gas sample probe, is attached to the waveguide at this point. The primary assembly

---

[23] P. P. Woskov, K. Hadidi, P. Thomas, K. Green, G. Flores, and D. A. Lamar, Field Test of a Real-Time Calibrated Microwave Plasma Continuous Emissions Monitor for Stack Exhaust Metals, p. 4.

has three tangentially mounted jets through which a carrier gas flows. These jets add vorticity to the bulk axial flow drawn through the probe, and the resultant flow has streamlines in a helical pattern. This helicity serves to confine the plasma in the chamber. Figure 3.2 shows the formation of the helical streamlines in the plasma chamber.
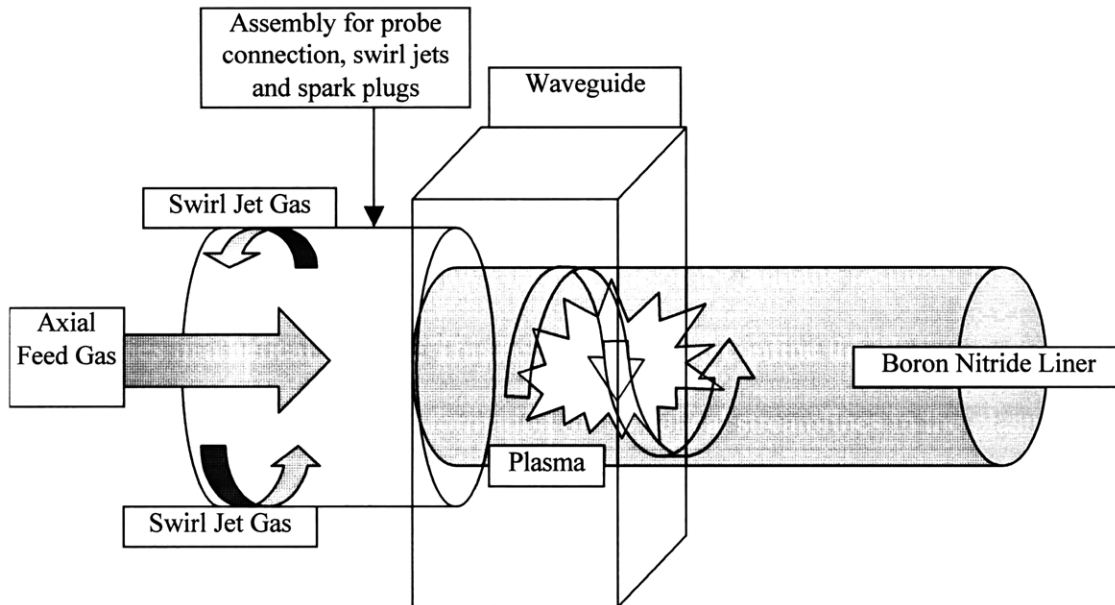

Figure 3.2 Formation of Helical Streamlines for Plasma Confinement

There is another assembly that is mounted on the other side of the waveguide. This second assembly supports the length of the boron nitride not supported by the waveguide, and is used to mount the exhaust system to the plasma chamber.

In addition to the swirl jets, the primary assembly houses the spark plugs used to create an initial plasma breakdown. The spark plugs are connected to a 15kV neon sign transformer to create initial free electrons in the flow when the voltage is discharged through the spark plugs. These free electrons interact with the electric field in the plasma chamber, and cause breakdown in the feed gas, creating the plasma.

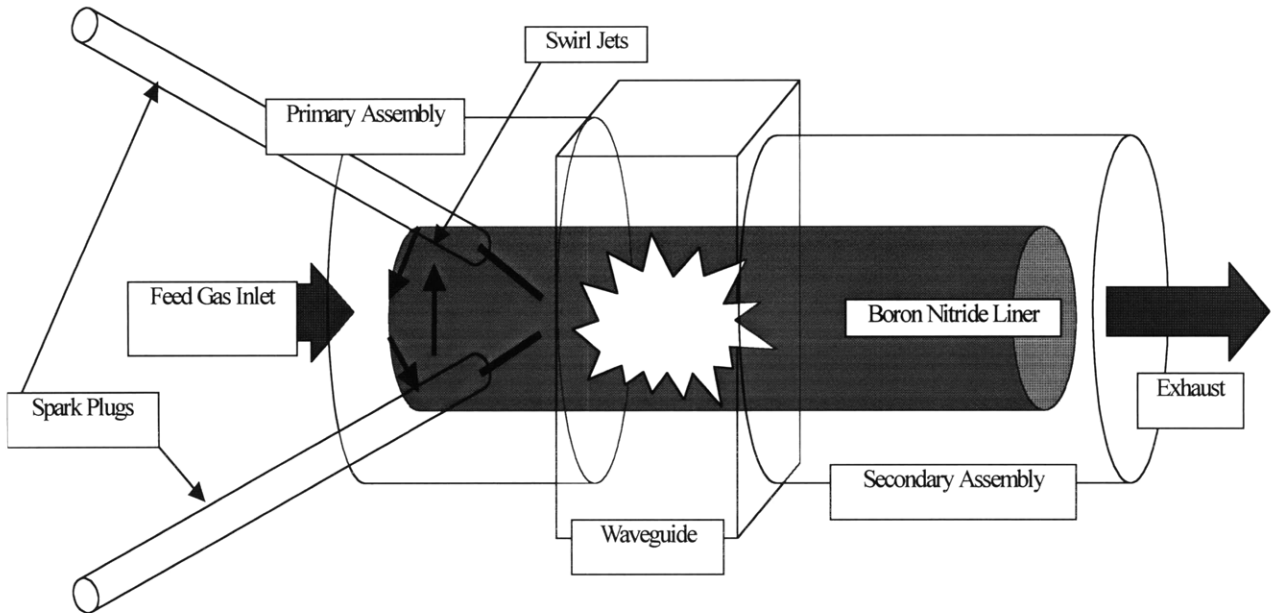A complete diagram of the waveguide and assemblies is shown in Figure 3.3.

Figure 3.3 Complete Waveguide and Assemblies

3.2 Nebulizer Setup

The calibration approach will use an attached source of known metals' concentration that can periodically inject these metals into the gas sample line. Figure 3.4 shows the overall outline for the nebulizer system setup.
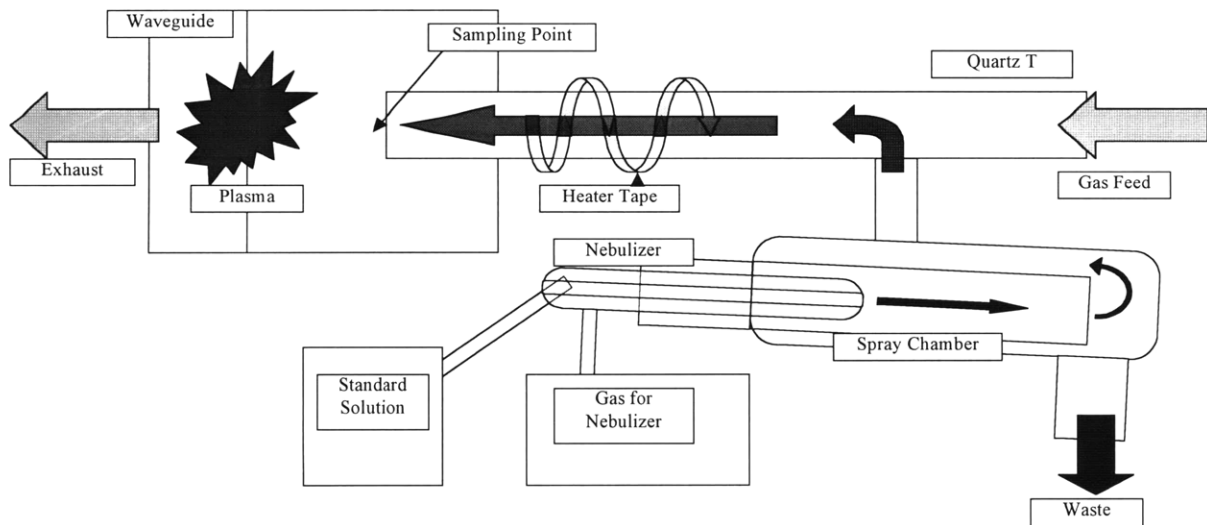

Figure 3.4 Physical Setup of the Nebulizer System

The torch utilizes a 5/16-inch I.D. sample probe that connects through a quartz "T", 10 inches in total length, into the plasma chamber. This "T", also 5/16 inch I.D., extends into the plasma chamber from the tip of the KF-25 joint until it is approximately 4 ¼ inches from the base of the waveguide. Heater tape surrounded the KF-25 joint and the short arm of the quartz "T", keeping the temperature of the "T" approximately 200 °C. This point, 4 ¼ inches from the base of the waveguide, is what is referred to as the sampling point. In addition, the next two inches are marked into ¼-inch segments, and it is at these positions that the rod insertions were done. The segments were measured with respect to the quartz "T", so that a measurement at 0 inches refers to the position where the quartz "T" enters the plasma chamber. A measurement at 1 inch refers to the point one inch further into the chamber, closer to the plasma. See Figure 3.5 for a more detailed description.
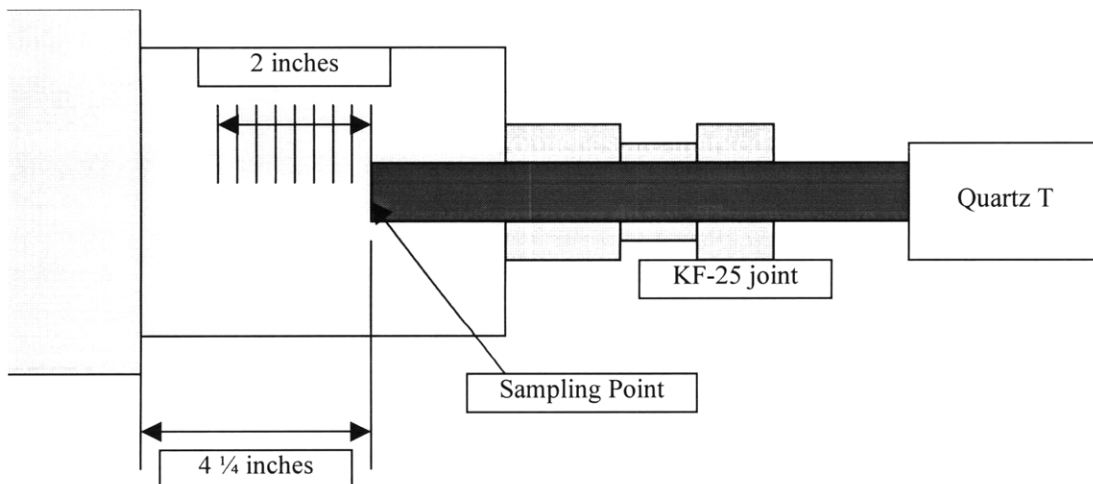

Figure 3.5 Close-up of Sampling Point and Quartz T Insertion

The calibration source is connected to the branch line of the quartz "T". The calibration source for this work will be a Minehard pneumatic nebulizer that aerosolizes a standard solution containing a known concentration of the metals. The standard solution is pumped and aspirated by a high-pressure gas through the nebulizer, causing the liquid

to become an aerosol. As this is occurring, there is suction applied through the quartz

"T," in the direction of the gas flow, to draw a gas sample through the plasma. This

suction causes a small fraction of the aerosol in the spray chamber to travel up the short

arm of the "T" and make its way to the plasma. In this manner, a known concentration of

metals can be introduced into the plasma for calibration purposes, although most of the

solution impacts the sides of the spray chamber and collects in the waste flask set up at

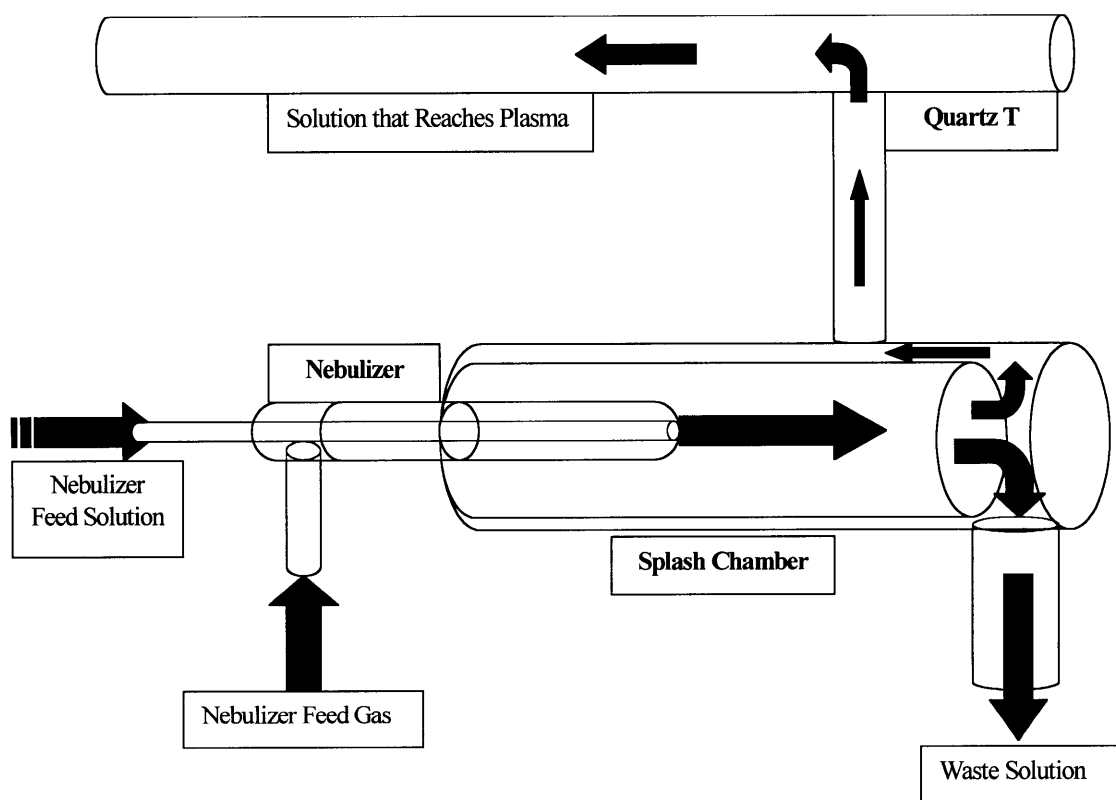the end. Figure 3.6 shows a magnification of the nebulizer and splash chamber.

Figure 3.6 Close-up of the Nebulizer and Splash Chamber

3.3 Alumina Rods

In order to insert known amount of masses near the plasma, a novel approach was

designed and implemented. Initially, solid 4-mm alumina (99.7 % Al_2O_3) rods were used

as a surface to place the metal solutions. The solutions would be pipetted onto the face of

the rod and allowed to dry, leaving the metal behind. The rod would then be placed in a

centering jig to prevent the rod from impacting the sides of the quartz "T", and inserted to the correct position. Figure 3.7 shows the centering jig and the input side of the quartz "T".
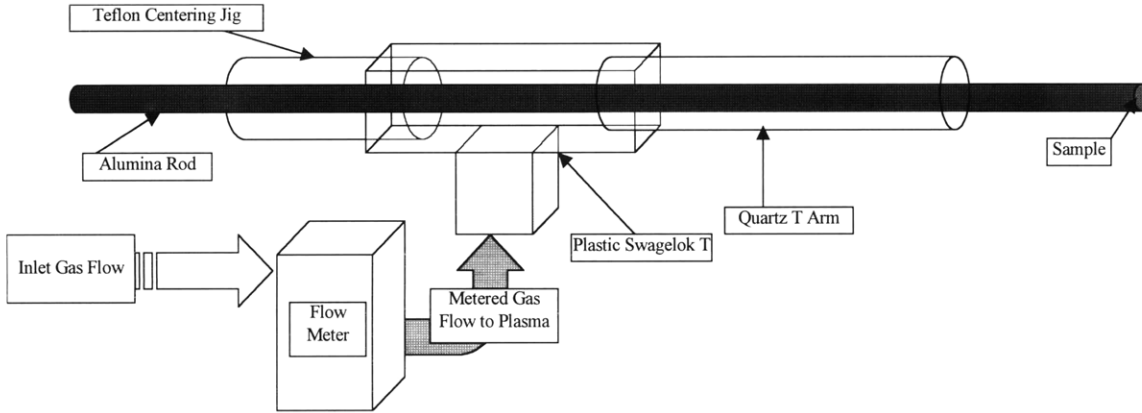

Figure 3.7 Centering Jig and Alumina Rod Setup

However, it was difficult using a solid alumina rod as a surface to boil off the lead solution at positions other than two inches from the sampling point. The plasma could not heat the surface adequately enough to boil off the sample without sliding the rod in further to verify the mass had indeed been boiled off, invalidating the test. So another approach was used. Hollow alumina rods, with 1-mm holes bored into them, were used in place of the solid rods. The rods were the same outer diameter, 4-mm. Tungsten wire, 0.1-mm in diameter, was bent into a single loop, and the loop ends were threaded into the hollow alumina rods, so the loop was 0.5 inches from the surface of the alumina rod, as shown in Figure 3.8
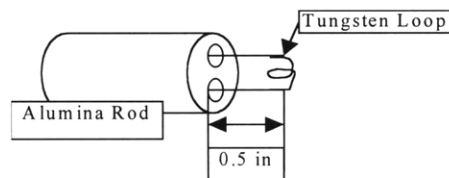

Figure 3.8 Placement of Tungsten Loop in Alumina Rod

This ends the description of the physical setup of the plasma torch, the nebulizer setup, and the alumina rod specifications. Figure 3.9 gives the dimensions of the main components used.
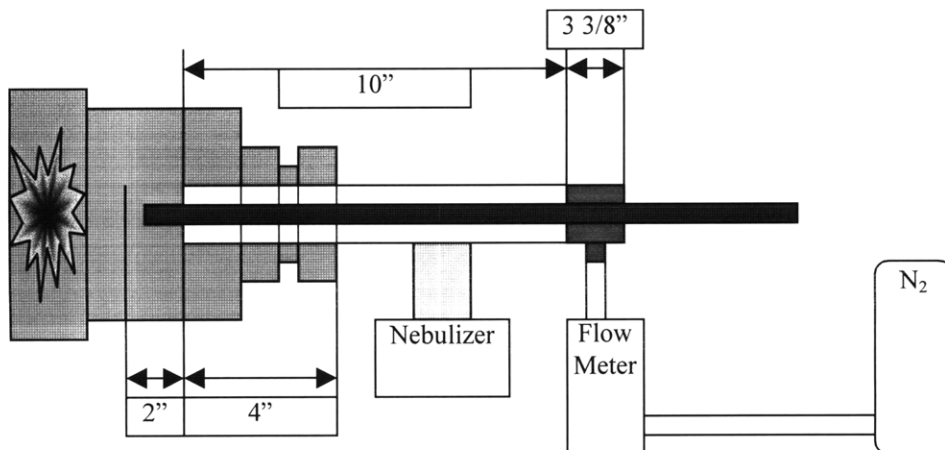

Figure 3.9 Measurements of the Physical Setup

3.4 Spectrometer System and Software Setup

The spectrometer used for the measurements was a Jarrell-Ash 0.5-m MonoSpec 50 scanning monochromator with a 2400 groove/mm grating. The light was reflected onto a 2048 element CCD detector array from StellarNet, Inc.

The software used was SpectraScope, also from StellarNet, Inc. This software allowed the user to monitor up to six different history channels, which were each programmed to monitor specific peaks, such as the lead 405.787-nm peak. The software was set for an ADC (analog-digital conversion) rate of 200 kHz, with an integration time of 20 msec. This provided an adequate number of points in the lead signal to sum over.

4.0 Calibration

4.1 Motivation

As stated earlier, the nebulizer is connected to a standard solution source. The source solution is aspirated by high pressure gas through the nebulizer, causing the liquid to become an aerosol. As this is occurring, there is a gas flow going through the quartz "T" to draw gas into the plasma. This causes a small fraction of the aerosol in the spray chamber to travel up the short arm of the "T" and find its way into the plasma. The analyte mass contained in this aerosol solution for a given integration time, m_{nebpl}, is the mass of metal present in the plasma over the time of integration. It will be determined by comparing the intensity of light received from this initially unknown mass to a signal intensity received from a known mass, m_{direct}, on a directly inserted rod placed on or near the sample input to the plasma chamber, as shown in equation 4.1.

$$
\begin{aligned}
m_{direct} &\propto \int I_{direct} dt \\
m_{nebpl} &\propto \int I_{nebpl} dt \\
m_{nebpl} &= m_{direct} \times \frac{\int I_{nebpl} dt}{\int I_{direct} dt}
\end{aligned}
\qquad (4.1)
$$

The mass transport efficiency, η, is equal to m_{nebpl} divided by the analyte uptake into the nebulizer, m_{nebtot}. The total mass of sample nebulized is equal to the volume flowrate of the nebulizer, $\dot{V}$ [ml/min], multiplied by the solute density of the sample solution, ρ [μg/ml], and the time sampled, Δt [min]. All of these quantities are known or measured directly. Having determined m_{nebpl}, the efficiency is obtained by dividing m_{nebpl} by m_{nebtot}, shown in equation 4.2. This is the efficiency of the aerosol reaching the plasma as a function of geometry and flow characteristics, but determined experimentally.

$$\eta \equiv \frac{m_{nebpl}}{m_{nebtot}} \qquad (4.2)$$

But why determine the nebulizer efficiency in the first place? The answer is that in the field, the researcher may not be able to do direct rod insertions, and certainly not if the waveguide is placed inside of the exhaust duct. Also, the rod-inserted samples are shown to be highly reproducible, and the nebulizer performance also repeats itself well. The nebulizer system can be connected to the plasma system in any test, and can be used as a means of calibration. For instance, in a field test, the condition for isokinetic sampling would determine the torch exhaust velocity, v_{sl}. What is sought is ρ_{test}, or the concentration of mass in the test flow. The measured quantity would be the intensity, I_{test}, which is proportional to ρ_{test}.

Now the researcher has to calibrate the system. From lab experiments, the researcher has a value of the efficiency for the position of the sampling point and for the particular gas flow through the torch, so η is known. The calibration solution concentration ρ_{neb}, the nebulizer flow rate $\dot{V}$, and the time interval of calibration Δt_{neb} are all given or measured directly. The researcher then runs the system with the calibration solution, and notes an intensity I_{nebpl} due to the calibration solution. This intensity relates to the mass m_{nebpl}, not m_{nebtot}. With the calculated efficiency, the researcher can determine m_{nebpl} from the known quantities, as shown in equation 4.3.

$$m_{nebpl} = \eta \times m_{nebtot} = \eta \dot{V} \rho_{neb} \Delta t_{neb} = I_{nebpl} \Delta t_{neb} \qquad (4.3)$$

where ρ_{neb} is given in equation 4.4.

$$\rho_{neb} = \frac{m_{nebpl}}{v_{sl}\Delta t_{neb}} \qquad (4.4)$$

With the test complete, the researcher can calculate the desired quantity, ρ_{test}.

$$\rho_{test} = \rho_{neb} \times \frac{I_{test}}{I_{nebpl}} \qquad (4.5)$$

In this way the researcher would determine the concentration of mass in an airstream given the flow conditions and test specifications.

4.2 Effects of Solution Concentration on Signal Intensity

The effect of solution concentration versus signal has been documented in the lab. Tests were done in which lead and chromium solutions with concentrations ranging from 10 μg/ml up to 10,000 μg/ml were used to record the signal strength. As seen in Figure 4.1 on the next page, the response of the detector, and hence the plasma, is mostly linear for the concentrations tested, with some non-linearity at low concentrations. The curves are straight-line fits on a log-log plot to the experimental points. Hence, the assumption was made that any arbitrary solution concentration chosen would not affect the calculation of the nebulizer efficiency. Since the intensity response is linear, then this assumption is valid.
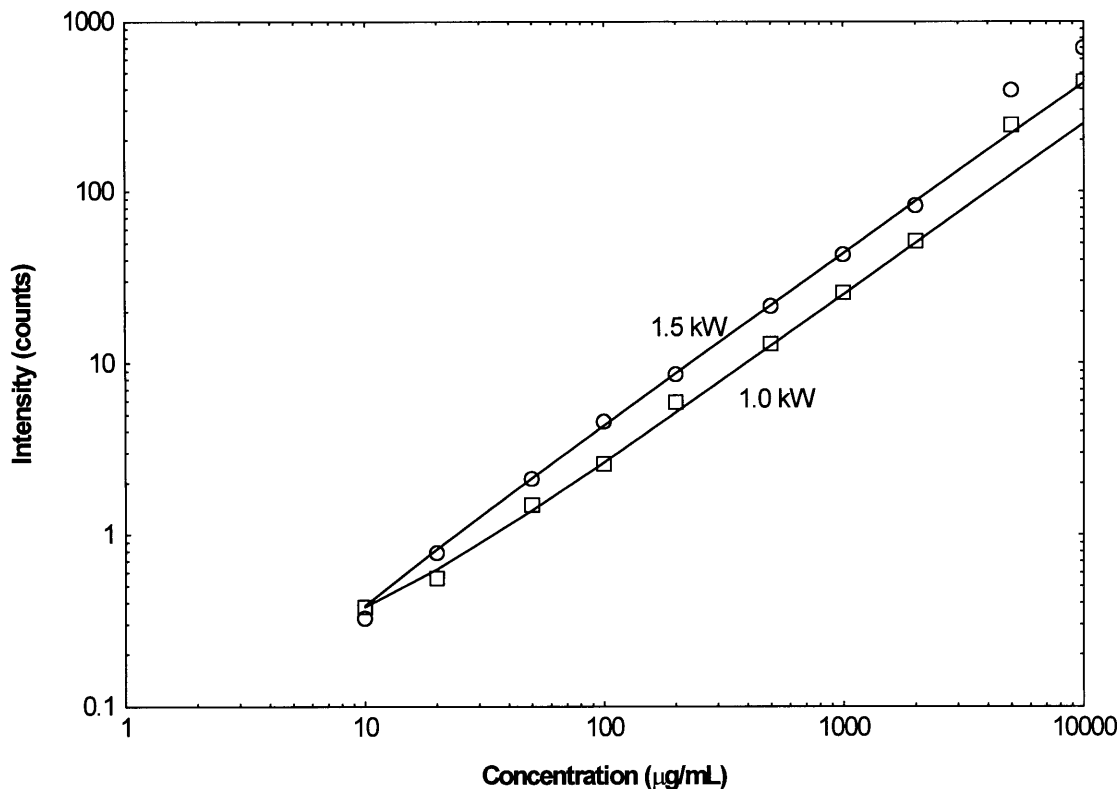
Figure 4.1 Intensity vs. Concentration of Nebulizer Solution for Lead

4.3 Experimental Procedure

Once the tungsten loop was secured, it was placed near the heater tape used to heat the input feed gas. Stock solutions of 10,000-μg/ml lead in 5% HNO_3 were diluted to concentrations of 2000-μg/ml for use in the tests. Then 5-μl drops were placed on the loop with a precision micropipette, and the solution was allowed to dry, leaving the lead on the tungsten loop. Once the lead solution had crystallized on the loop, the alumina rod was placed into the centering jig in the quartz "T" with the opposite end of the rod going in first to eliminate contamination. The rod was then positioned for the analysis, and the data was taken. Detector counts were taken in a continuous history mode, in which the detector sent a signal to the computer at a rate of 200 kHz. The data was outputted as an intensity versus time trace.

However, it was soon discovered that tungsten oxidized violently in the plasma when air was used as the feed gas. The amount of light produced by the oxidizing tungsten would easily overload the sensitive detectors, and rendered them useless in searching for the lead signals. Instead, nitrogen was used as the feed gas, and as the swirl jet gas. Nitrogen allows the tungsten loop to incandesce without oxidizing violently, and further allowed a more controlled boil off of the lead particulates. The pressure regulator on the nitrogen bottle was set to the proper pressure by attaching a flowmeter to the end of the nitrogen line and opening the regulator until the flowmeter read 30 SCFH (Standard Cubic Foot per Hour). This value was chosen to mimic the actual sample line volume flow rate of 27.55 SCFH used in the EPA test. Then the pump on the system was matched to the probe flow as to mimic isokinetic sampling, a main requirement for this type of analysis. This stabilized the plasma, and minimized the fluctuations of signal due to pressure and flow mismatches in the plasma chamber.

5.0 Analysis

Once the data was collected, the analysis began. Intensity versus time plots of the

lead 405.78-nm peak, a tungsten peak located near the lead peak, and three background

pixels were used to calculate the analyte mass transport efficiency. Using the rod tests,

the light signal was integrated over the time it took the lead to boil off of the tungsten

filament. Below is a data file for lead on a tungsten loop in a nitrogen plasma 0.5 inches
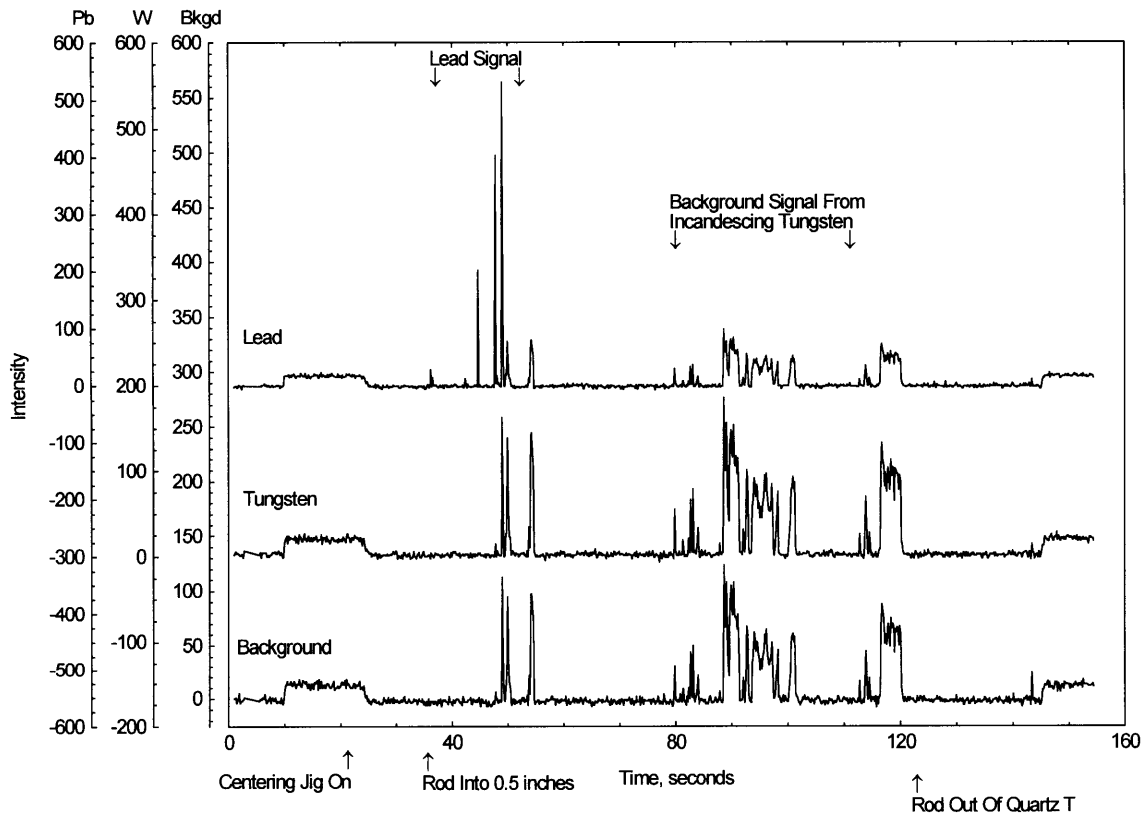
from the sampling point.

Figure 5.1 Intensity vs. Time Plot of Lead Signal at 0.5 Inches from Sampling Point

The first step in the data analysis comes in determining the background average of the

noise to correct the signal. The background pixel closest to the lead signal was averaged

over the time the centering jig was in place (27 seconds), to the time the rod was inserted

(36 seconds), and an average value, b_{avg}, was obtained. This pixel was chosen by

inserting a tungsten rod into the plasma, and picking a pixel that did not rise in intensity.

41

That way, any excess signal the tungsten may cause the lead peak signal to increase by can be screened out. The background was then subtracted from the lead signal, and the corrected intensity was summed to determine the total intensity of signal proportional to 5μl of 2000 μg/ml lead solution inserted into the plasma, as shown in equation 5.1.

$$I_{int\,eg}^{direct} = \sum_{t=t_i}^{t_f}\left(I_t - b_{avg}\right) \qquad (5.1)$$

Because of the nature of the rod tests, the lead signal was not long lived. At most, there were on the order of 10 different points to sum up, with the signal quickly dropping to the average background levels once the rod was in place. The computer sampled data at a rate of 200 kHz, with an integration time of 20 msec. This rate was extended from 55 kHz initially, since there were not enough points being collected at the lower frequency to justify this approach. The sampling rate versus pixel intensity is shown below.
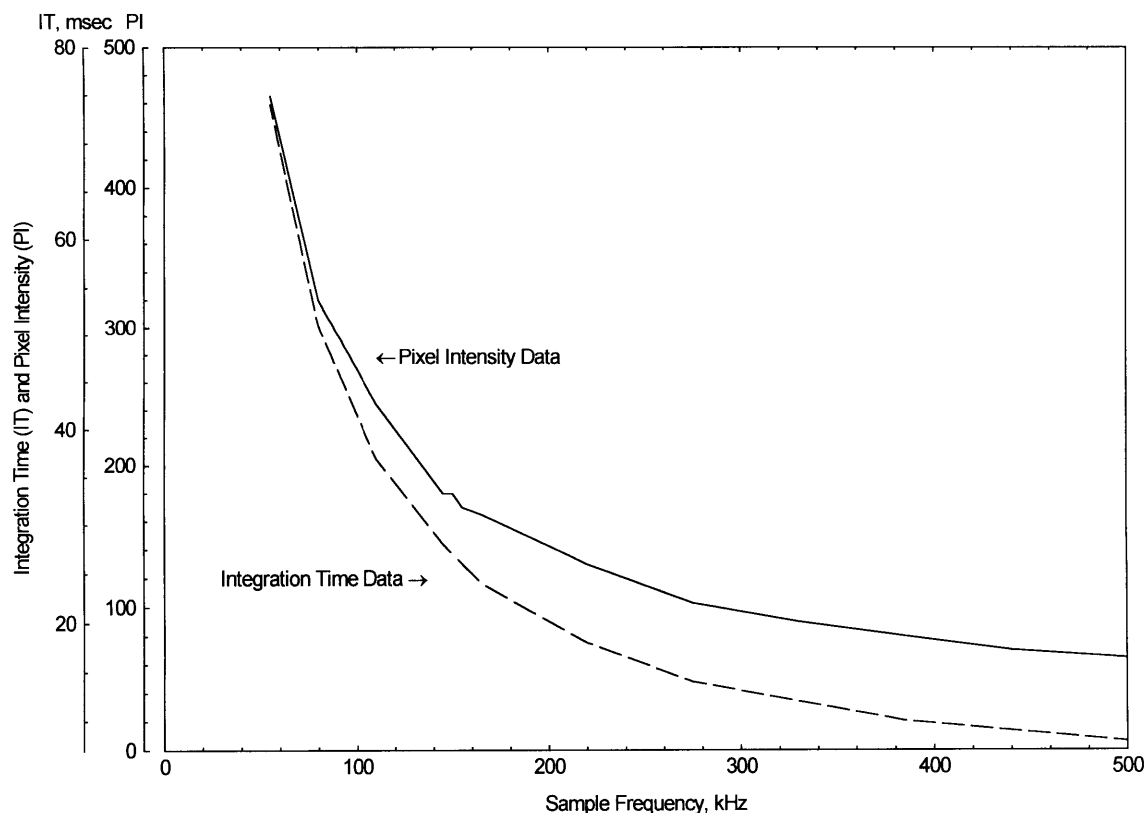

Figure 5.2 Pixel Intensity and Integration Time vs. Sample Frequency

The pixel intensities range from 465 counts/pixel at the lowest sampling frequency of 55 kHz, to 60 counts/pixel at the highest sampling frequency, 550 kHz. The integration times ranged from 74 msec at 55 kHz to 7 msec at 550 kHz. However, since both the rod and nebulizer signal are affected in the same way, the nebulizer efficiency does not depend on sampling frequency.

Once $I_{int\,eg}^{direct}$ has been calculated, $I_{int\,eg}^{neb}$ is obtained next. By taking careful note in the logbook of when events took place, the calculation of $I_{int\,eg}^{neb}$ is rather straightforward. Below is the nebulizer file taken immediately after the data for lead on a tungsten loop at 0.5 inches from the sampling point in a nitrogen plasma.
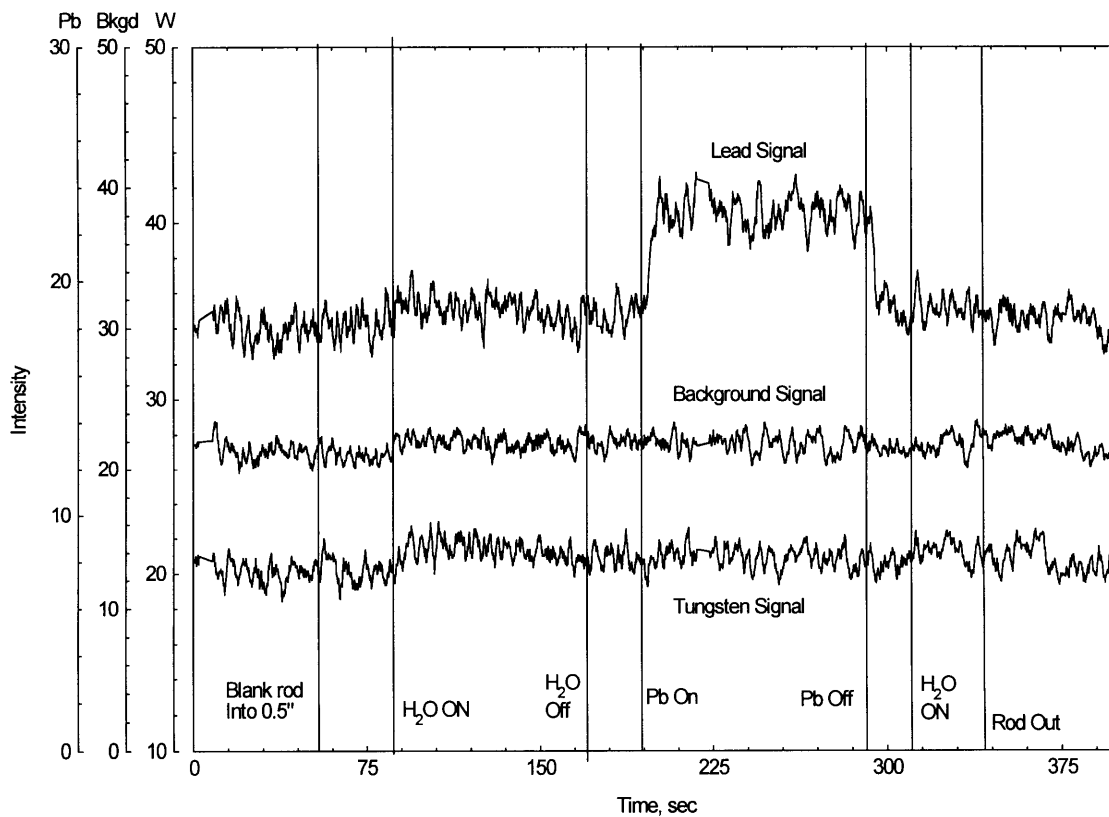

Figure 5.3 Nebulizer Intensity vs. Time

The figure above also demonstrates the effect of the rod and water on the signal. For instance, the average signal intensity from the start until the insertion of the blank rod

43

is 21.31 counts. The average for the next time interval, with only the rod perturbing the flow is 20.99 counts. And finally, the average for the water and rod perturbation is 21.97 counts. These small perturbations by the blank rod and clean water were noticed in all of the nebulizer files, and were corrected. The increase in signal from the water vapor coming from the splash chamber alone is consistent with pervious work done in determining the effect of moisture on the plasma.[24]

In much the same manner, $I_{int\,eg}^{neb}$ is calculated from the raw data. First, the background average, b_{avg}, is calculated, using the data from when the blank rod is inserted and the deionized water is turned on. The signal is summed over the time the nebulizer is aspirating lead, and the intensity is found using equation 5.2.

$$I_{int\,eg}^{neb} = \sum_{t_i}^{t_f} \left(I_t - b_{avg} \right) \qquad (5.2)$$

Now that $I_{int\,eg}^{neb}$, $I_{int\,eg}^{direct}$, and m_{direct} are known, m_{nebpl} can be calculated. For the time interval t_f - t_i = Δt that the nebulizer signal was summed, m_{nebtot} is calculated as given in the previous chapter. Then the efficiency η is calculated by taking the quotient of m_{nebpl} over m_{nebtot}, as shown in equation 4.2. The efficiencies were plotted as a function of relative rod position, Figure 5.4, and a straight line was fitted to the points. As the rod is pushed further into the plasma chamber, the lead boil off is not subject to the same loss mechanisms as the lead aspirated from the end of the sample line. In order to subject the lead boil off to the same loss mechanisms, the rod must be pushed back to the end of the sample line. However, it is difficult to achieve complete lead boil off is at rod positions close to the end of the sample line, <0.5 inches. So the efficiencies were

---

[24] S. E. Long, and R. F. Browner, <u>Influence of Water on Conditions in the Inductively Coupled Argon Plasma</u>, p. 1465-1466

calculated at positions that the boil off could be determined, and the value at the sampling
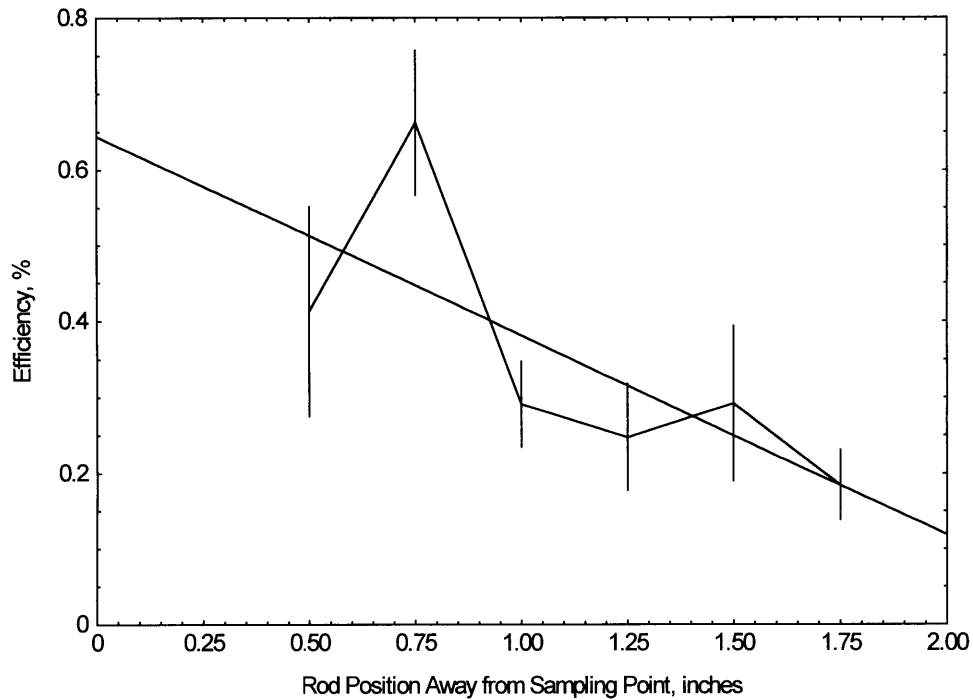
point extrapolated.

Figure 5.4 System Efficiency as a Function of Relative Rod Position

Extrapolating to the sampling point, the nebulizer system has an efficiency of

0.644 ± 0.153 % at the sampling point. In a recent field test against EPA Method 29, a

value of 0.5 % was used. However, this value was uncorrected for the gas temperature.

The temperature of the gas at the flowmeter was 128 °F and 400 °F in the sample line. In

the field test, a span calibration of 92 mg/acm (actual cubic meter) gave good agreement

with Method 29 results, and is given in equation 5.3

$$S = \frac{\eta \times m_{nebtot}}{V} \qquad (5.3)$$

where S is the span calibration, and V is the volume of gas in sample line. Now, the true

gas flowrate is given by equation 5.4

$$SCFM_{true} = \frac{SCFM_{read}}{\left(\dfrac{SG(T_o)14.7}{1.0(P_o)530}\right)^{\frac{1}{2}}} \qquad (5.4)$$

where

SCFM$_{true}$ is the true gas flow rate,

SCFM$_{read}$ is the reading on the flowmeter,

SG is the specific gravity of the gas at STP (air = 1.0),

T$_o$ is the operating temperature, °R (°F + 460), and

P$_o$ is the operating pressure, PSIA (PSIG + 14.7).

With the operating conditions at the field test, the flowmeter correction becomes

$$SCFM_{true} = \frac{SCFM_{read}}{1.053} \qquad (5.5)$$

using P$_o$ as atmospheric pressure.

However, the span calibration is in acm, not dscm. There is another temperature

and moisture correction for converting from acm to dscm, given as equation 5.6.

$$acm = \frac{dscm(100 - mole\%H_2O)(293)}{100(273 + T)} \qquad (5.6)$$

For the test conditions, mole%H$_2$O was ~6.0, and T was 400 °F, or 204 °C. Combining

these factors gives another correction factor of dscm = 1.73 acm.

So, combining these corrections, the corrected efficiency, for constant m$_{nebtot}$, is

$$\eta' = \frac{S'V'\eta}{SV} = \frac{1.73\eta}{1.053} \qquad (5.7)$$

where the primed variables are the corrected values, all in dscm, which are the

uncorrected factors multiplied by these new constants. The value of the corrected

efficiency being 0.821 %, which is 22 %greater than the extrapolated value. This is in

good agreement with past work done to measure the efficiency of a Minehard nebulizer, which was determined to be in the range of 0.5 % to 1.5 %.[25]

The following table gives the calculated efficiencies for the various rod positions, as well as the average and standard deviation of the average values.

Efficiencies, in %						
Distance from Sampling Point	Run 1	Run 2	Run 3	Run 4	Run 5	Run 6
0"	Cannot Resolve Lead Data at These Positions					
0.25 "	Cannot Resolve Lead Data at These Positions					
0.5 "	0.168518	0.415994	0.295477	0.259266	na	0.436801
0.75 "	0.684299	0.638978	0.420528	0.616037	na	0.952622
1.0 "	0.451951	0.23688	na	0.182105	0.214622	0.325419
1.25 "	0.122159	0.190752	0.130424	0.196059	0.454661	0.392725
1.5 "	0.157843	0.120589	0.284718	0.175093	0.487123	0.652171
1.75 "	0.171099	0.127639	0.170993	0.151637	na	0.117709
Distance from Sampling Point	Run 7	Run 8	Run 9	Run 10	Average	St.Dev.
0"	Cannot Resolve Lead Data at These Positions					
0.25 "	Cannot Resolve Lead Data at These Positions					
0.5 "	0.312867	na	na	na	0.41318	0.276023
0.75 "	na	na	na	na	0.662493	0.19099
1.0 "	na	0.428798	0.19851	na	0.291184	0.111992
1.25 "	na	na	na	na	0.247797	0.140918
1.5 "	na	0.495394	0.187152	na	0.29194	0.203628
1.75 "	na	0.368858	na	na	0.184656	0.09287

Table 5.1 Efficiency Calculations for each Rod Position

However, these efficiencies were calculated in a plasma with 0.5-cfm nitrogen flowing through the quartz "T". How does the efficiency change with other flows, or

---

[25] D. D. Smith, and R. F. Browner, <u>Measurement of Aerosol Transport Efficiency in Atomic Spectrometry</u>, pp. 533-537.

even in an air plasma? As a preliminary answer to these questions, three other tests were done at 1.75 inches from the sampling point. Two tests used solid alumina rods in air and nitrogen plasmas at 0.5-cfm probe flow, and the other used a tungsten filament in a nitrogen plasma at 1.0-cfm flowing through the quartz "T". The results are given below.

Test Procedure	Efficiency, %
Pb on W Loop in N_2 Plasma: 0.5 cfm	0.185 ± 0.093
Pb on W Loop in N_2 Plasma: 1.0 cfm	0.193 ± 0.154
Pb on Al_2O_3 Rod in Air Plasma: 0.5 cfm	0.300 ± 0.018
Pb on Al_2O_3 Rod in N_2 Plasma: 0.5 cfm	0.046 ± 0.009

Table 5.2 Effects of Different Testing Parameters on Efficiency at a Given Position

Judging from the numbers, the efficiency is more sensitive to gas composition and rod makeup than flow changes. Doubling the flow rate only yielded a 4.43 % increase in the efficiency. However, changing the gas composition and rod makeup yielded a much larger increase of the efficiency at the same flow rate. Figure 5.5 shows the boil off of the lead sample on a solid Al_2O_3 rod in an air plasma. The lead sample takes much longer to boil off than with the tungsten loop in place, referred in figure 5.1. This increase time may be the key as to the increased efficiency of the solid Al_2O_3 rod in an air plasma.
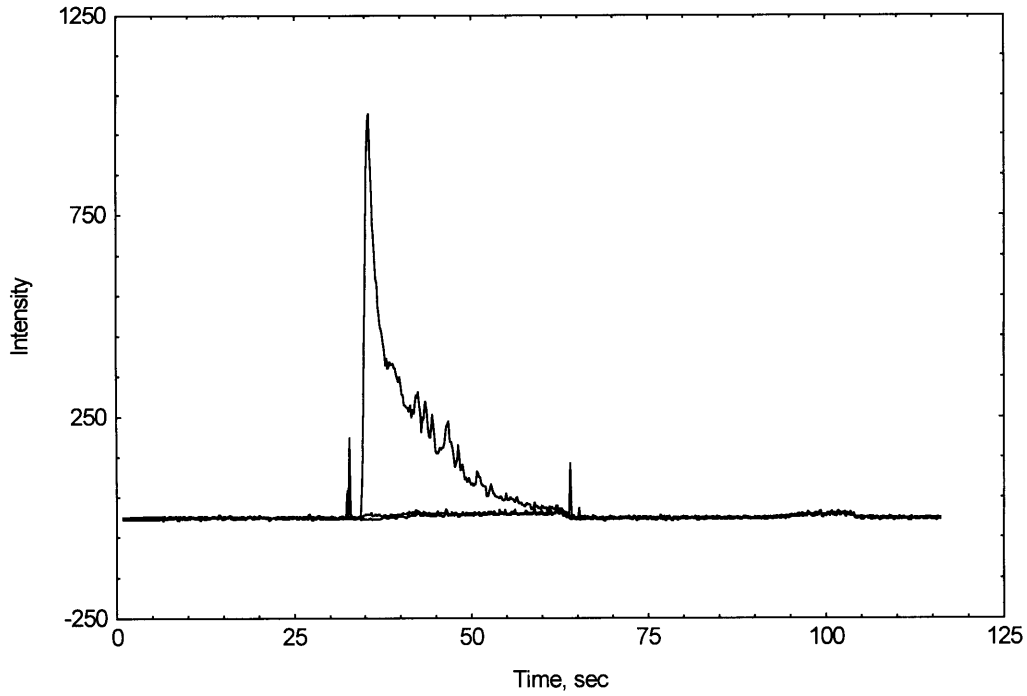
Figure 5.5 Boil-Off of Lead Sample from a Solid Al$_2$O$_3$ Rod in an Air Plasma

Also presented is a time trace of the boil-off of the lead sample from a solid Al$_2$O$_3$ rod in
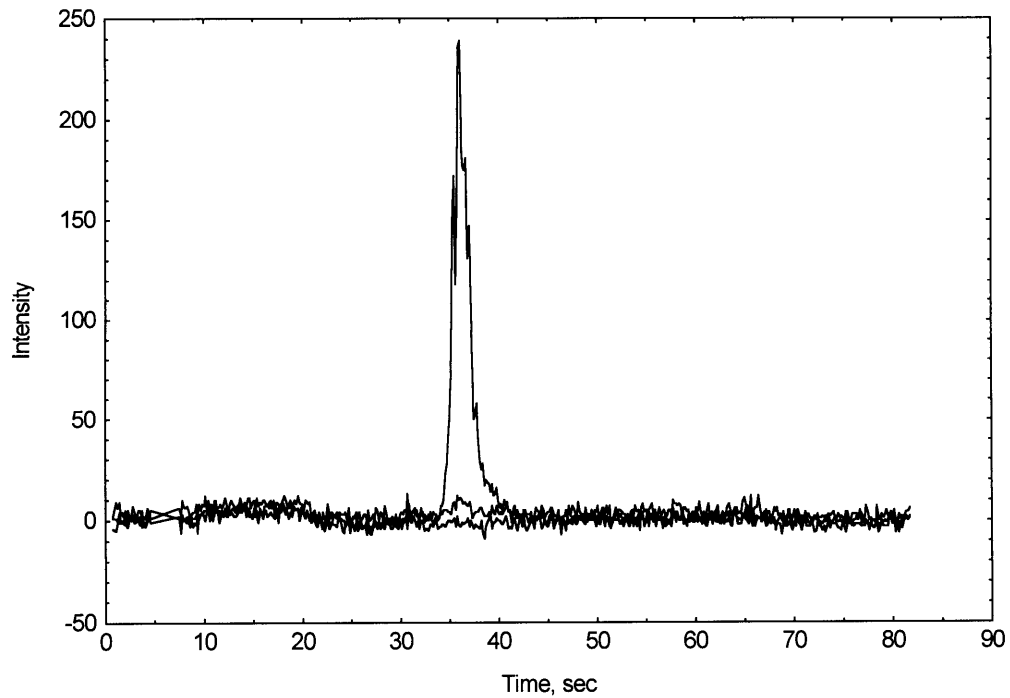
a nitrogen plasma.

Figure 5.6 Boil-Off of Lead Sample from a Solid Al$_2$O$_3$ Rod in a Nitrogen Plasma

The sample in nitrogen has a shorter boil off time than the air sample, and that may be the reason for the large difference in the solid Al_2O_3 data. A longer boil off time would lead to a greater heating of the rod, and a greater possibility that more of the sample would completely boil off. However, the nebulizer data for the Al_2O_3 rod in N_2 plasma test is not conclusive, because the intensity of the lead signal is not much greater than the background, which is not the case for the other tests. In those cases, the lead signal was clearly evident over the background for the same sample line flow rate and standard solution concentration. This test should be attempted again to verify this conclusion.

6.0 Conclusions and Recommendations for Future Work

6.1 Conclusions

Direct rod insertions of samples are a viable method of calculating the nebulizer transport efficiency for calibrating the MIP system. By varying the relative rod position of the sample insertion, the efficiency can be extrapolated by a straight-line fit of the rod efficiencies. This method has several advantages:

1) The transport efficiency does not depend on the standard solution concentration. The solution concentration can be chosen such that the signal from the nebulizer is optimal without changing the efficiency.

2) The MIP can be set to the precise operating conditions as it would be subjected to in the field, and the calibration done at those conditions. The only change would be the rod perturbing the plasma, but these perturbations can be accounted for and corrected.

6.2 Recommendations for Future Work

The effect of moisture on the calibration must be understood. The direct rod tests should be repeated with the nebulizer aerosolizing water in the plasma to determine the impact of moisture on the efficiency.

One other recommendation that is being implemented as this thesis was written is the use of a Gelman Science Type A/E glass fiber filter to determine the efficiency. The quartz T is attached to a base that houses the filter. The flow is set, and the nebulizer is activated. The filter collects the mass of sample sent through the T, and is sent off to the

lab for analysis. There are some questions about the flow characteristics that must be answered, but this method will serve as a check to the direct rod calibration.

Moisture again is a key component to the calibration. The effects of dry particles in the plasma versus an aerosol should be determined. Particle size should also be studied. Will the efficiency change for larger particles ($>20\mu m$) in diameter versus small particles ($<1\mu m$) in diameter? The feed gas composition should be further studied. The large discrepancy of the initial alumina tests in air and nitrogen should be verified to determine if the feed gas composition has a major impact on the transport efficiency.

As the push to commercialize the torch continues, it may become necessary to do fundamental research on the plasma itself in order to aid in the understanding of the influence the plasma has on the transport efficiency, if at all. Although there is more work that needs to be done on the MIP before commercialization becomes a reality, this calibration is a step in the right direction. This innovative way to determine the transport efficiency can be done in a relatively easy manner, and is straightforward in its approach. The fair agreement of the rod insertions with the EPA field test data also suggests this method is viable in determining the nebulizer transport efficiency for the MIP.

7.0 References

Cited :

1) French, A. P., and Taylor, E.F., "An Introduction to Quantum Physics", ch. 1, W W Norton & Company Inc., New York, © 1978 MIT.

2) Long, S.E., and Browner,R.F., Influence of Water on Conditions in the Inductively Coupled Argon Plasma, *Spectrochimica Acta*, Vol. 43B, No. 12, pp. 1461-1471, 1998.

3) Pollack, Brian, Establishing Isokinetic Flow for a Plasma Torch Exhaust Gas Diagnostic for a Plasma Hearth Furnace, SM Thesis, Nuclear Engineering & Mechanical Engineering, MIT, 1996.

4) Smith, D.D., and Browner,R.F., Measurement of Aerosol Transport Efficiency in Atomic Spectrometry, *Analytical Chemistry*, Vol. 54 No. 3, pp.533-537, March 1982.

5) U. S. EPA, Method 5, Determination of Particulate Emissions from Stationary Sources, 40 CFR 60 Appendix A, July 1995.

6) U. S. EPA, Method 29, Determination of Metals Emissions from Stationary Sources, 40 CFR 60, Appendix A, April 1996.

7) U. S. EPA, Revised Standards for Hazardous Waste Combustors, Performance Specification 10 – Specifications and Test Procedures for Multi-Metals Continuous Monitoring Systems in Stationary Sources, 61 FR 17499 – 17502, April 19, 1996.

8) Woskov,P.P., Hadidi,K., Thomas,P., Green,K., Flores III,G., and Lamar,D.A., Field Test of a Real-Time Calibrated Microwave Plasma Continuous Emissions Monitor for Stack Exhaust Metals, PSCF Report PSFC/RR-98-1, February 1998.

Non-Cited :

9) Bratzel Jr.,M.P., Dagnall,R.M., and Winefordner,J.D., A New, Simple Atom Reservoir for Atomic Fluorescence Spectrometry, *Analytica Chimica Acta*, Vol. 48, pp. 197-203, 1969.

10) Canals,A., Hernandis,V., and Browner,R.F., Evolution of Drop Size Distributions for Pneumatically Generated Aerosols in Inductively Coupled Plasma-Atomic Emission Spectrometry, *Spectrochimica Acta*, Vol. 45B, No. 6, pp. 591-601, 1990.

11) Chauvin,J.V., Newton,M.P., and Davis,D.G., The Determination of Lead and Nickel by Atomic Absorption Spectrometry with a Flameless Wire Loop Atomizer, *Analytica Chimica Acta*, Vol. 65, pp. 291-302, 1973.

12) Lund,W., and Larsen,B.V., The Application of Electrodeposition Techniques to Flameless Atomic Absorption Spectrometry, Part I. The determination of Cadmium with a Tungsten Filament, *Analytica Chimica Acta*, Vol. 70 pp. 299-310, 1974.

13) Matusiewicz, Henryk, Thermal Vaporisation for Sample Introduction in Microwave Induced Plasma Analytical Emission Spectrometry, *Specrtochimica Acta*, Vol. 13, No. 1, pp. 47-68, 1990.

14) Sharp, Barry L., Pneumatic Nebulisers and Spray Chambers for Inductively Coupled Plasma Spectrometry, A Review, Part 2. * Spray Chambers, *Journal of Analytical Atomic Spectrometry*, Vol. 3, pp. 939-962, October 1998.

15) Sychra,V., Kolihová,D., Vyskocilová,O., Hlavác,R., and Püschel,P., Electrothermal Atomization from Metallic Surfaces. Part 1. Design and Performance of a Tungsten-tube Atomizer, *Analytica Chimica Acta*, Vol. 105, pp. 263-270, 1979.

16) Woskov,P.P., Rhee,D.Y., Thomas,P., Cohn,D.R., Surma,J.E., and Titus,C.H., Microwave Plasma Continuous Emissions Monitor for Trace Metals, PSFC Report PFC/JA-96-10, March 1996.